ACS APPLIED BIO MATERIALS

www.acsabm.org

Article

# Long-Term Culture of Stem Cells on Phosphate-Based Glass Microspheres: Synergistic Role of Chemical Formulation and 3D Architecture

Dhanak Gupta, Kazi M. Zakir Hossain, Martin Roe, Emily F. Smith, Ifty Ahmed, Virginie Sottile,* and David M. Grant*

Cite This: *ACS Appl. Bio Mater.* 2021, 4, 5987−6004

Read Online

ACCESS | Metrics & More | Article Recommendations | Supporting Information

**ABSTRACT:** Phosphate-based glasses (PBGs) are biomaterials that degrade under physiological conditions and can be modified to release various ions depending on end applications. This study utilized slow-degrading (P45:45$P_2O_5$-16CaO-24MgO-11$Na_2O$-4$Fe_2O_3$, mol %) and comparatively faster degrading (P40:40$P_2O_5$-16CaO-24MgO-20$Na_2O$, mol %) PBG microspheres with or without porosity, to evaluate the combined effect of chemical formulation and geometry on human mesenchymal stem cells (MSCs), a clinically relevant cell source for orthopedic applications. Scanning electron microscopy showed 2, 46, and 29% of P45 bulk (P45-B), P40 bulk (P40-B), and P40 porous (P40-P) microspheres, respectively, that had cracks or peeling off surfaces after 42 days of incubation in culture medium. Cytotoxicity assessment showed that glass debris released into the culture medium may interact with cells and affect their survival. Direct-contact cell experiments up to 42 days showed that P45-B microspheres did not sustain viable long-term cell cultures and did not facilitate extracellular matrix formation. On the other hand, P40-B microspheres enhanced alkaline phosphatase activity, calcium deposition, and collagen and osteocalcin production in MSCs. Introduction of porosity in P40 glass further enhanced these parameters and proliferation at later time points. The small pore windows (<5 $\mu$m wide) and interconnection (<10 $\mu$m wide) may have allowed limited cell penetration into the porous structures. P40-B and P40-P have potential for bone repair and reinforcement therapy based on their chemical formulation and porous geometry.

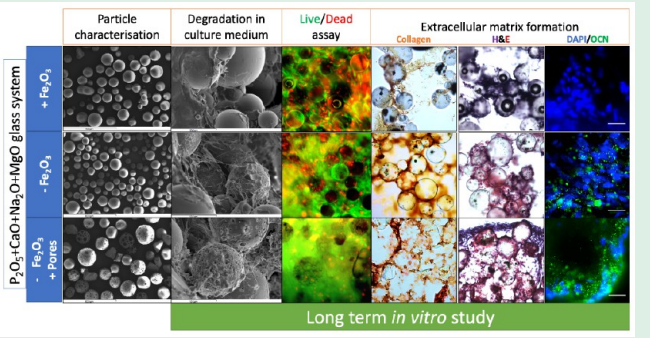


**KEYWORDS:** *phosphate-based glass, porosity, mesenchymal stem cells, microspheres, osteogenic differentiation*



## 1. INTRODUCTION

Human mesenchymal stem cells (MSCs) from the bone marrow are a prime source of stem cells for bone tissue engineering and regenerative applications. Pre-seeding of implants with MSCs or their differentiated progeny has been shown to improve the response to implantation in vivo,[1] and therefore, a range of MSC-based clinical trials for bone- and cartilage-related diseases have been undertaken worldwide.[2]

The mechanisms regulating MSC differentiation into bone-forming cells involve chemical cues, soluble factors,[3] and environmental factors such as mechanical stimuli,[4] microgravity,[5] and substrate geometry and topography.[6] For instance, the presence of porosity (pore sizes > 100 $\mu$m in diameter) in bone implants is known to be beneficial for bone ingrowth and osteointegration in vivo.[7] It enables nutrient transport and cell migration,[8] and the surface curvatures trigger molecular pathways favorable for osteogenic differentiation.[9]

Several porous scaffolds derived from natural, synthetic, or composite materials such as polymers, metals, and ceramics have been developed for bone repair applications.[10] Silica-based bioactive glasses (such as 45S5 Bioglass) are unique in the way that they form a carbonate hydroxyapatite layer on glass due to glass dissolution under physiological conditions, which enables faster bone bonding at the bone−implant interface compared to other bioceramics.[11] Implantation of 13−93 bioactive glass porous scaffolds pre-seeded with MSCs has been shown to support tissue infiltration and bone formation in a rat model.[12]

**Received:** February 1, 2021
**Accepted:** May 6, 2021
**Published:** July 29, 2021

Phosphate-based glasses (PBGs) are a form of silica-free bioactive glass that is widely investigated. These glasses are formed from inorganic phosphate-network linkages between the $PO_4^{3-}$ tetrahedral units, and oxides such as $Na_2O$, MgO, CaO, $Fe_2O_3$, $TiO_2$, and SrO can be introduced into the network to vary degradation rates, associated ion release, and bioactivity of the glass material under physiological conditions. This tunable nature makes PBGs attractive candidates for biomedical applications.[13]

For bone tissue engineering applications, recent studies using PBGs have focused on complex ternary, quaternary, and quinary glass systems formulated to contain higher amounts of P and Ca, similar to the inorganic component of bones, hydroxyapatite.[14] These studies investigated in vitro degradation profiles (including mass loss and/or ion release) of PBGs lasting between 15 and 504 days; however, the in vitro cytocompatibility investigations were typically much shorter, between 2 and 21 days[15−36] (see the Supporting Information S1, Table S1). This limits the understanding of how glass degradation could affect cell growth and differentiation over longer periods in situ.

More recently, porous and non-porous PBG microspheres (MSs) with the chemical formulation of $40P_2O_5$-16CaO-4MgO-(20-$x$)NaO-$x$$TiO_2$ mol % ($x$ = 0 or 2.5%) and $40P_2O_5$-(16-$x$)CaO-24MgO-20NaO-$x$SrO ($x$ = 0, 4, 8, 12, and 16 mol %) were reported to support the culture of MSCs up to 12 days[16] and 14 days,[27] respectively, and also supported new bone formation in a sheep bone defect model after 13 weeks.[37]

This study explores how the chemical formulation and geometry (porous or non-porous) of these PBG MSs might affect the response of human MSCs over extended culture periods, for as long as 6 weeks, exploring the cytocompatibility of these bioactive glass materials for biomedical applications.

## 2. MATERIALS AND METHODS

**2.1. Manufacture of Glass MSs.** Two different particle morphologies were used to study cellular responses: smooth bulk MS (P40-B) and porous MS (P40-P) of the same composition were compared. In addition, two compositions of bulk MS were also compared to evaluate the composition and degradation influence: P40-B and P45-B (Table 1). MS size was kept constant between

**Table 1. Nominal Glass Compositions (mole %) Used in This Study**[a]

| glass | $P_2O_5$ | CaO | MgO | $Na_2O$ | $Fe_2O_3$ | $SiO_2$ | $B_2O_3$ | $Al_2O_3$ |
|---|---|---|---|---|---|---|---|---|
| P45 | 45 | 16 | 24 | 11 | 4 | 0 | 0 | 0 |
| P40* | 40 | 16 | 24 | 20 | 0 | 0 | 0 | 0 |
| BSG# | 0 | 1.7 | 0 | 7.1 | 0 | 78.6 | 9.5 | 3.1 |

[a]*Fe is absent in P40 formulation, #composition from Samco, UK.

batches, and a non-degradable borosilicate glass (BSG) control was included in the study.[38] PBGs were manufactured using the following precursors: $NaH_2PO_4$, $CaHPO_4$, $MgHPO_4$, $P_2O_5$, and $Fe_2O_3$ (Sigma-Aldrich, U.K.). The precursors were weighed and dried in a Pt/5%Au crucible at 350 °C for 30 min in a furnace and then melted and held at 1150 °C for 90 min for P40 composition and at 1280 °C for 2 h for P45 composition. The molten glass was then poured onto a steel plate and allowed to cool down to room temperature (RT). Then, the cooled glasses were grounded into microparticles using a Retsch PM100 milling machine and sieved into varying sizes ranging from 63 to 125 μm. Bulk and porous glass MSs were produced from these microparticles via flame spheroidization utilizing a thermal spray gun (Metallisation Ltd, UK) as previously described.[16] Post manufacture, the MSs were sieved into desired sizes ranging from 63 to 125 μm. Borosilicate glass MSs (BSG) in a similar size range were produced by crushing standard laboratory glass vials (Samco, UK), followed by the same flame spheroidization process. In total, two batches of BSG, three batches of P45-B, three batches of P40-B, and two batches of P40-P were used in this study.

**2.2. Major Axis Length, Sphericity, and Pore Measurements of the MSs.** The MSs were mounted on aluminum stubs using carbon adhesive tabs and sputter-coated with approximately 15 nm of gold. The samples were then examined in a JEOL 6400 scanning electron microscope using the secondary electron (SE) imaging signal at a beam voltage of 20 kV. Scanning electron microscopy (SEM) images were thresholded to remove the background; the major axis length (MAL) and sphericity of particles in at least five fields of view were measured using Image J 1.48t (see Supporting Information S3, Figures S1 and S2). MSs at the edge of the images or overlapping MSs were not selected for quantification. For the porous MS ($n$ = 22), incomplete pore windows on the edges of the image or wrongly identified pore windows were also not selected for quantification. The internal porous structure of MSs was examined using a FEI Quanta 200 3D (FEI, Portland, OR) equipped with a Quorum PPT 2000 (Quorum Technologies Ltd, Loughton, UK) cryostage and an in-house custom-built sledge. SE and backscattered electron (BSE) images were acquired at a beam voltage of 15 kV and current setting of 0.14 nA. Ion milling was performed at 20 kV with currents between 1 nA and 30 pA. The ion beam distance was set at 15 mm with 3.5 as spot size, and all sections were cut at a tilt angle of 52°.

**2.3. Surface Area Analysis, Relative Density, and Tapped Density.** The surface area was measured using a Micromeritics ASAP 2420. Multipoint Brunauer−Emmett−Teller (BET) was performed at a constant temperature of 77.4 K, using krypton as the adsorbate. The samples were outgassed at 300 °C under high vacuum for 12 h to remove moisture and other adsorbed gases and then analyzed from 0.06 to 0.27 relative pressure ($P/P_o$) at −167 °C in liquid nitrogen. Isotherms were analyzed using Microactive V4.03.01 software to calculate BET specific surface areas.

Relative density was measured using a Micromeritics AccuPyc 1330 gas pycnometer (Norcross, GA, USA). Before measuring the density of samples, a straight-line equation was plotted between the true volume and measured volume values using an empty container (with zero true volume) and a reference sphere (of known true volume). Once the measured volume values of the samples were obtained, the true volume values were calculated using the straight-line equation formed earlier. The density of the sample was then calculated by dividing the true volume by the mass of sample, weighed using a 4-decimal place-sensitive balance (Ohaus Analytical standard AS 200) and normalized to the density of water at the temperature of the pycnometer.

The tapped density was measured using a Quantachrome Autotap machine.[39] Samples of known mass were added to a container, which was tapped until the height of the sample in the container became constant (100 taps). The final volume was used to calculate the tapped density of the sample.

**2.4. Energy-Dispersive X-ray Spectroscopy (EDS) in the SEM.** Samples were embedded in a cold-setting epoxy resin, which were ground on silicon carbide discs and polished with cloths down to 1 μm. The polished blocks were then coated by vacuum evaporation with a conductive layer of 20 nm of carbon. Elemental analysis was performed in the Philips (FEI) XL (30)-w scanning electron microscope using an Oxford Instruments INCA energy-dispersive X-ray microanalysis system using a beam voltage of 20 kV and a working distance of 10 mm utilizing the BSE imaging signal. Appropriate standards used for elemental analysis were jadeite (for Na), gallium phosphide (for P), wollastonite (for Ca), MgO (for Mg), and pyrite (for Fe). The electron beam current was optimized with the spot size control in order to obtain a minimum X-ray acquisition rate of 4000 counts/s.

**2.5. Incubation of MSs in Water.** Two experiments were performed to study the effect of hydration on MSs. In one


https://doi.org/10.1021/acsabm.1c00120
ACS Appl. Bio Mater. 2021, 4, 5987−6004

experiment, MSs were incubated in ultrapure water (Milli-Q) for 24 h and left overnight to dry in a cell culture hood. Samples were gold-coated and examined in the JEOL 6400 scanning electron microscope. In another experiment, samples were examined in an uncoated state and observed in a Philips XL30 FEG environmental scanning electron microscope. Images were captured before flooding the chamber with water to fully submerge the samples for 15 min. Images were captured at 15 kV in the wet mode to study morphological changes. This was followed by a second flood cycle for 1.5 h, and images were again captured.

**2.6. Incubation of MSs in Culture Medium for 42 days to Assess Morphological Changes.** The MSs were prepared in the same way as for cell culture, as detailed in Section 2.7.1. Briefly, they were cleaned with 70% industrial methylated spirit (IMS, SLS, UK), dried overnight, washed with phosphate-buffered saline (PBS), and washed with culture medium, before finally transferring them to 200 $\mu$L of culture medium for 42 days. The resulting material-to-medium ratio was approximately 20 mg:1 mL for bulk MSs and 10 mg:1 mL for the porous MS. Medium changes were performed after 1 day and then subsequently every 2−3 days, up to 42 days of incubation. At each time point, culture medium was removed, and MSs were collected from wells and then Au-coated and examined in the JEOL 6400 scanning electron microscope using standard operating conditions. Five fields of view were captured for each MS type at every time point at 100× magnification. MSs with cracks or with peeling off surfaces were manually counted per field of view (see the Supporting Information S3, Figure S3), and morphological changes were presented as the percentage of MSs in a sample with apparent cracks or peeling off surfaces.

**2.7. Cytocompatibility Studies.** The cytocompatibility studies were divided into two main categories: cell−material direct interactions and cell−material indirect interactions. Reagents were purchased from Thermo Fisher Scientific unless otherwise stated.

*2.7.1. Human MSC Culturing.* Adult immortalized human bone marrow-derived MSCs and green fluorescent protein (GFP)-expressing MSCs were used in this study, as previously described.[40] The cells were cultured in standard culture (SC) medium containing Dulbecco's modified Eagle medium (DMEM) supplemented with 10% (v/v) fetal calf serum, 1% (v/v) non-essential amino acids, 1 mM L-glutamine, and 0.5% (v/v) penicillin/streptomycin and maintained at 37 °C in a humidified atmosphere with 5% $CO_2$.

*2.7.2. Cell Seeding on MSs for Direct-Contact Assessments.* MSs were assumed to have a nominal size distribution of 100 $\mu$m. Using their tapped density measurements, MS types were weighed such that the particles formed a monolayer at the bottom of a 96-well plate before seeding with cells.[38] The weighed MSs were first cleaned with IMS for 2 h at a constant agitation of 30 rpm, before air drying overnight in a cell culture hood. Particles were then washed three times with PBS and three times with SC medium, before 30 min of incubation at RT in SC medium. At this stage, the MSs were transferred to wells previously coated with 100 $\mu$L of a 10 mg/mL solution of poly(2-hydroxyethyl methacrylate) (pHEMA, Sigma-Aldrich) solution in 95% ethanol to obtain ultra-low cell attachment conditions on the 96-well flat-bottom plate (for preferential attachment of cells to MSs only), where they formed a single layer at the bottom of the well. Finally, the medium was carefully removed and replaced with the cell suspension (200 $\mu$L per well). The samples were further agitated at 45 rpm for 5 min at RT, followed by 30 min of static incubation at 37 °C and 5% $CO_2$. This regime was repeated five times before undisturbed incubation at 37 °C and 5% $CO_2$ overnight. The medium change was performed 24 h after cell seeding and subsequently every 2−3 days for the length of the experiment.

*2.7.3. Cytotoxicity Evaluations for Indirect-Contact Assessments.* For all cytotoxicity evaluations, MSs were cleaned with IMS for 2 h and then washed three times with PBS and three times with SC medium before 30 min of incubation in SC medium. Then, the medium was removed and replaced with fresh culture medium at 37 °C and 5% $CO_2$ based on an ISO standard for irregular-shaped porous devices (ISO 10993-12:2009)[41] and ISO standard for tests for in vitro cytotoxicity (ISO 10993-5:2009).[42] Three different cytotoxicity experiments were performed, as described in the Supporting Information S2.

*2.7.4. Cell Metabolic Activity Assay.* Cell metabolic activity was measured using a PrestoBlue assay. Briefly, medium was removed and cells were washed with PBS before adding 200 $\mu$L of PrestoBlue working solution (1:9 reagent/warm Hanks balanced salt solution) to each test well and three blank wells. Cells were then incubated at 37 °C and 5% $CO_2$ according to the manufacturer's instructions. During the exponential phase of the reaction, 100 $\mu$L of reaction solution was transferred to a clear 96-well plate, and fluorescence reading was measured at 530 nm excitation and 590 nm emission filters on a Tecan Infinite M200 microplate reader (Tecan, UK). Cell metabolic activity was expressed after removing the value for the unreduced (blank) reagent and normalizing to the reaction time.

*2.7.5. DNA Content Assay.* All samples were lysed by three cycles of freeze thawing at −80 °C and 30 min of sonication using the Bioruptor, Diagenode, USA. The cell lysates were then diluted (1 in 100 in Tris-EDTA buffer), and 100 $\mu$L of samples was added to a 96-well plate. The DNA content was quantified using the Quant-i PicoGreen double-stranded DNA assay kit according to the manufacturer's instructions. Fluorescence intensity readings were taken on a Tecan Infinite M200 microplate reader at 480 nm excitation and 520 nm emission.

*2.7.6. Fluorescein Diacetate/Propidium Iodide Staining.* At each time point, cells were washed with PBS, and then, DMEM containing 8 $\mu$g/mL fluorescein diacetate (FDA, Merck Millipore, UK) and 20 $\mu$g/mL propidium iodide (PI) (Sigma-Aldrich) was added. Cells were incubated at RT for 5 min in the dark and then incubated in DMEM only for imaging. Images were acquired using a Nikon TS100 inverted fluorescent microscope. Images ($n \geq 4$) were used to quantify red and green fluorescence signals on days 1 and 4 of culture using Image J. Percentage cell viability was calculated by dividing the green pixels by total pixels (green + red) in the same field of view. As the number of cells on the MS increased over time, they caused progressive aggregation of neighboring MSs, forming larger 3D aggregates, which could be imaged at day 21 using a Leica TCS LSI confocal macroscope.

The abovementioned technique enabled visualization of live/dead cells only at the bottom and top layers (facing toward the bottom and lid of the well plate, respectively) of 3D aggregates. To visualize cell viability inside the 3D aggregates, GFP-MSCs were seeded on MSs, and on day 21, cells were stained with 20 $\mu$g/mL PI for 5 min before fixing in 4% paraformaldehyde in PBS at 4 °C for 10 min. Samples were then cryo-sectioned (Section 2.7.7) and visualized using a ECLIPSE 90i fluorescent Nikon microscope.

*2.7.7. Sectioning of 3D Aggregates.* Fixed 3D aggregates were washed with PBS for 5 min and immersed in a 15% sucrose solution in PBS overnight. Samples were embedded in OCT medium and sectioned (20 $\mu$m section size) at a cryostat chamber temperature of −20 °C. The sections were dried overnight at RT and stored at 4 °C before Sirius Red staining, hematoxylin and eosin (H&E) staining, and osteocalcin immunostaining.

*2.7.8. Neutral Red Uptake Assay.* A stock solution of Neutral Red (NR, 0.2 g/L) (Sigma-Aldrich) was further diluted to 1:80 ratio in DMEM as a working solution, which was syringe-filtered using a 0.2 $\mu$m filter to remove crystals. For cell viability assessment, the medium was removed and the cells were washed with PBS before adding (100 $\mu$L/well in 96-well plate) NR dye medium to test wells and three blank wells. After 3 h of incubation at 37 °C and 5% $CO_2$, the NR medium was discarded, and the cells were washed with PBS. At this stage, images were taken using a Nikon Eclipse TS100. For quantification, a desorbing solution (49% ethanol, 1% glacial acetic acid, and 50% water) was added to the cells (same volume as used for NR dye medium), and after 10 min, at RT, absorption was measured at 540 nm using a Tecan Infinite M200 microplate reader. Cell viability was expressed as NR uptake after removing blanks and normalizing to the control medium for each time point. A viability of less than 70% was considered to be cytotoxic, as outlined by the ISO standard for biological evaluation of medical devices (ISO 10993-5:2009).[42]



https://doi.org/10.1021/acsabm.1c00120
ACS Appl. Bio Mater. 2021, 4, 5987−6004

**Table 2. Summary of MAL and Sphericity Measurements of MSs**

| | | MAL | | | sphericity | |
|---|---|---|---|---|---|---|
| MS | *n* | mean ($\mu$m) | median ($\mu$m) | Shapiro–Wilk test ($p$ values) | mean | median |
| BSG | 632 | 90 ± 2 | 80 | <0.0001 | 0.83 ± 0.01 | 0.88 |
| P45-B | 634 | 90 ± 1 | 89 | <0.001 | 0.93 ± 0.01 | 0.98 |
| P40-B | 1046 | 85 ± 1 | 83 | <0.0001 | 0.92 ± 0.01 | 0.98 |
| P40-P | 385 | 114 ± 2 | 109 | <0.0001 | 0.88 ± 0.01 | 0.94 |

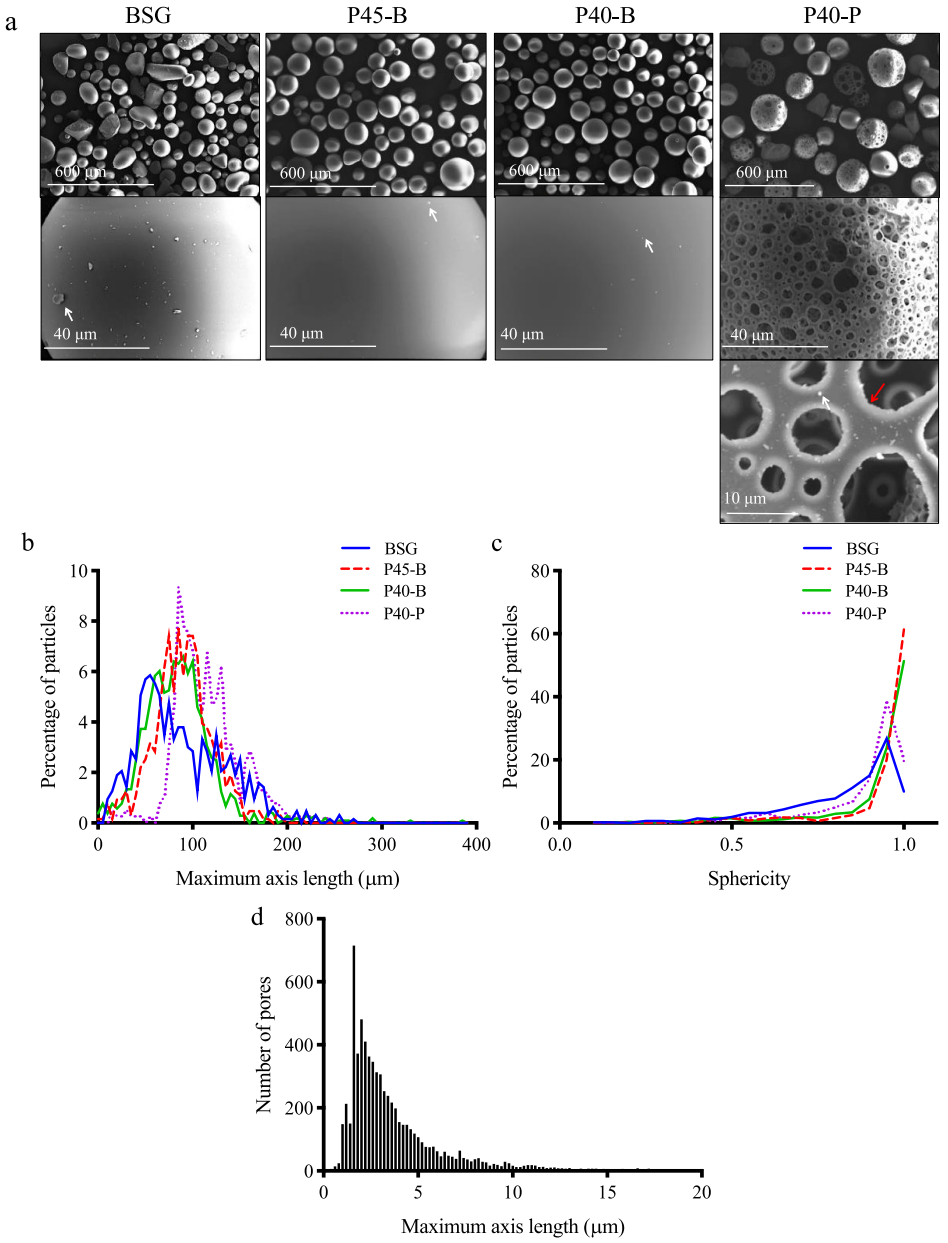


**Figure 1.** Morphology of different MS types. (a) MS as seen under SEM. White arrows indicate particulates deposited on the surface of MSs, and red arrows indicate shape pore edges in P40-P. (b,c) MAL and sphericity measurements of MSs assessed using SEM images. Bin sizes used for histograms were 5 and 0.05 $\mu$m, respectively. (d) MAL measurements of pore windows on the surface of P40-P. Bin sizes used for histograms were 0.2 and 0.01 $\mu$m, respectively. Notice that the vast majority of pores on P40-P have pore windows <5 $\mu$m.

*2.7.9. Alkaline Phosphatase Activity.* On specific time points, alkaline phosphatase (ALP) activity was measured using SIGMA-FAST *p*-nitrophenyl phosphate tablets (substrate) (Sigma-Aldrich). Briefly, 100 $\mu$L of cell lysates (or sterile distilled water for three blank wells) and 100 $\mu$L of substrate were added to a well, and after 20 min, absorbance at 405 nm was measured on a Tecan Infinite M200 microplate reader. The ALP activity is expressed as absorbance/$\mu$g of DNA after removing blanks and normalizing to the DNA content.

*2.7.10. Sirius Red Staining.* For staining, a working solution of 0.1% Sirius Red (Direct Red 80, Sigma-Aldrich) was prepared in 100 mL of saturated picric acid (Sigma-Aldrich). For qualitative assessment, sections of 3D aggregates were incubated in working solution for 30 min with occasional agitation every 10 min. The


https://doi.org/10.1021/acsabm.1c00120
ACS Appl. Bio Mater. 2021, 4, 5987–6004

Table 3. Surface Area, Density, and Surface Damage Measurements of MS

| MS | BET Surface area ($m^2/g$) | relative density | closed porosity (%)[a] | tapped density ($g/cm^3$) | tapped density normalized to closed porosity ($g/cm^3$) | time of maximum damage incurred during incubation in SC medium | MS with surface damage on day 42 (%) |
|---|---|---|---|---|---|---|---|
| BSG | 0.072 ± 0.013 | 2.20 ± 0.01 | 6.00 ± 0.01 | 1.13 ± 0.01 | 1.20 ± 0.02 | | 0 ± 0 |
| P45-B | 0.045 ± 0.013 | 2.57 ± 0.02 | 6.60 ± 0.02 | 1.30 ± 0.01 | 1.41 ± 0.03 | | 2 ± 1 |
| P40-B | 0.042 ± 0.012 | 2.61 ± 0.01 | 4.50 ± 0.01 | 1.31 ± 0.01 | 1.38 ± 0.02 | days 1−4, days 7−14 | 46 ± 3 |
| P40-P | 0.877 ± 0.134 | 2.42 ± 0.01 | 11.50 ± 0.01 | 0.54 ± 0.01 | 0.62 ± 0.02 | days 1−4, days 31−42 | 29 ± 3 |

[a]Relative density of BSG (Samco), P45, and P40[15] glasses is reported to be 2.34, 2.75, and 2.73 respectively. These values were used to calculate closed porosity. Error bars represent S.E.M.

excess stain was removed by blot drying, and samples were mounted using DPX before visualizing under an ECLIPSE 90i Nikon microscope. For quantification, intact 3D aggregates were washed twice with PBS and then fixed in 4% paraformaldehyde in PBS (4 °C) for 15 min before staining as described above. Samples were then washed with distilled water, and destaining solution (1:1 0.1 N NaOH/methanol) was added for 30 min with occasional agitation. Finally, 100 μL of extracts was used to measure absorbance at 540 nm using a Tecan Infinite M200 microplate reader. The background was removed from absorbance readings. Total collagen per sample was extrapolated using a standard curve prepared from rat tail collagen type 1 (Sigma-Aldrich), and values were normalized to the DNA content.

*2.7.11. X-ray Photoelectron Spectroscopy of 3D Samples.* Cells were seeded at 10,000 cells/$cm^2$, and on day 21 of culture, samples were fixed and washed with PBS and then with sterile distilled water. Samples were dried overnight at RT, and then, the top face of the 3D agglomerate samples was analyzed using the Kratos AXIS ULTRA with a mono-chromated Al K$\alpha$ X-ray source (1486.6 eV) operated at 10 mA emission current and 12 kV anode potential (120 W). Samples were mounted on a microscope slide with double-sided tape and then on the standard Kratos sample bar. Three wide (survey) scans were acquired for each sample, and high-resolution spectra for N 1s, C 1s, O 1s, P 2p, and Ca 2p were also assessed after charge correction to C 1s at 285 eV. The chamber pressure remained better than $5 \times 10^{-9}$ Torr after overnight pump down in the vacuum airlock. Charge neutralization was required as the samples were non-conducting. Data were processed using CasaXPS version 2.3.16 PR 1.6. The elemental atomic % at the surface region of the samples was estimated from the peak areas in the wide scans using Kratos RSFs. MSs without cells were included to validate specific signal quantification from cells or the extracellular matrix (ECM).[43] X-ray photoelectron spectroscopy (XPS) is a surface-sensitive technique, in which 95% of the photoelectrons come from three times the inelastic mean free path, that is, the majority of the signal is from the top few nm of the surface. Therefore, for samples with cells, only the cell surface or extracellular material was detected and not the underlying glass; therefore, any Ca and P detected can reasonably be assumed to be part of the biological material (Supporting Information S3, Figure S13). The N observed is from cell proteins, and therefore, it was used as a reference to compare Ca and P amounts that represented any hydroxyapatite-like material produced by the cells.

*2.7.12. Osteocalcin (OCN) Immunostaining.* Sections of 3D aggregates were permeabilized with 0.1% Triton X-100 in PBS for 40 min and then washed three times for 5 min with PBS before blocking with 3% goat serum (Sigma-Aldrich) in 1% bovine serum albumin (BSA, Sigma-Aldrich) in PBS for 30 min. After removing the blocking solution, the samples were incubated overnight with a rabbit polyclonal anti-osteocalcin primary antibody (Millipore), 1:200 dilution in 1% BSA in PBS, at 4 °C. Samples were then washed twice in PBS for 5 min and incubated in a 1:200 dilution in 1% BSA in PBS of Alexa Fluor 488 (green) goat anti-rabbit IgG at RT for 2 h before performing three 5 min PBS washes. Finally, samples were stained with 1 μg/mL Hoechst in 1% BSA in PBS for 15 min at RT, followed by three 5 min PBS washes, and then mounted using DABCO (1-4-diazabicyclo-2-2-2-octane) fluorescence mounting medium. Imaging was performed with an ECLIPSE 90i fluorescent Nikon microscope, with MS-only, primary antibody-only, and secondary antibody-only controls used to exclude the non-specific signal.

*2.7.13. Hematoxylin and Eosin Staining.* The sections of 3D aggregates were stained in hematoxylin for 5 min, washed, and then stained with eosin for 5 min. The samples were washed and dehydrated before mounting with dibutyl phthalate xylene and imaging under an ECLIPSE 90i Nikon microscope.

*2.7.14. SEM Sample Preparation and Characterization.* The 3D aggregates were first fixed in 4% paraformaldehyde in PBS (at 4 °C) and then incubated in 1% osmium tetroxide for 45 min at RT and then dehydrated. Before SEM examination, the samples were sputter-coated with Pt. SE images were acquired using the JEOL 6400 or Philips XL30 scanning electron microscope at electron beam voltages of 5−10 kV.

*2.7.15. Micro-CT Analysis.* Cells were seeded at 10,000 cells/$cm^2$ on P40-P and cultured for 7 days. On day 4, fresh medium containing barium sulfate (1.5 μL/mL) was added[44] (Supporting Information S3, Figure S4), and on day 7, cells were fixed in 4% PFA in PBS (at 4 °C) for 10 min. After washing with PBS, the cells were imaged under the XRADIA Versa XRM-500. Imaging was performed using the settings listed in the Supporting Information S1, Table S2.

*2.7.16. Statistical Analyses.* All statistical analyses were performed using IBM SPSS Statistics 22 and Prism Version 7.0d. Shapiro−Wilk test was used to test the normality of frequency MAL distribution of MSs and pore windows. The mean, standard deviation, and standard errors were computed for at least three replicate samples in all experiments. At least two independent experiments were performed for all cell culture studies, except cell viability analysis, which was run in a single measurement. For comparisons, ANOVA was performed. For pairwise comparisons, post-hoc analyses using least significant difference, equivalent to no adjustments, were carried out. $P$ values <0.05 were considered significant. For cytotoxicity assessment experiments involving spent media, a generalized linear mixed model was used, and DNA content of the cells present on the MS was considered as a random factor.

## 3. RESULTS

**3.1. Material Characterization.** The different PBG particles used in this study were initially characterized to determine their chemical and physical properties.

*3.1.1. Morphology of MSs.* The MAL and sphericity measurements are tabulated in Table 2. Typical morphology of all the MS is shown in Figure 1a. The mean and median MAL measurements showed all the bulk MS types were in a similar size range. However, there was an increase of nearly 30% in both mean and median MAL for the porous MS P40-P (Figure 1b). The distribution of all four types of MSs was not normal according to Shapiro−Wilk test. The bulk PBG MS (P40-B and P45-B) had a similar cumulative frequency distribution, while porous MS P40-P and BSG had an offset cumulative frequency distribution curve (Supporting Information S3, Figure S5).

The mean and median sphericity of all PBG MS (Figure 1c) was consistent at 0.9. However, BSG had a relatively lower



https://doi.org/10.1021/acsabm.1c00120
ACS Appl. Bio Mater. 2021, 4, 5987−6004

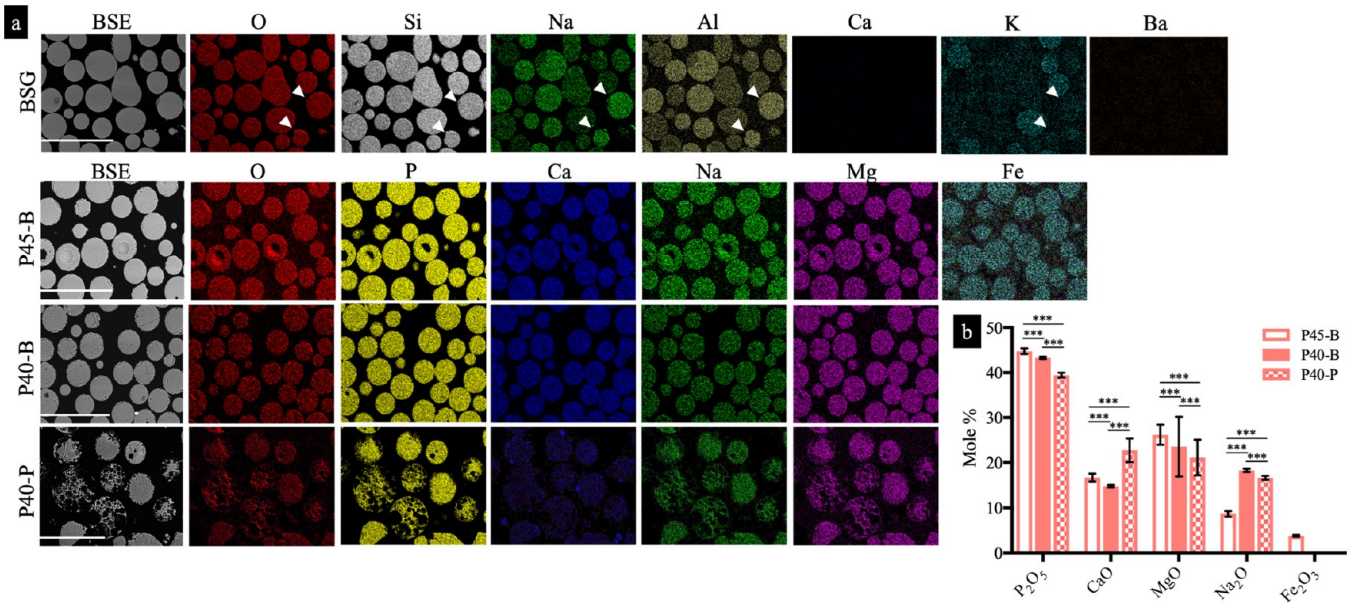


**Figure 2.** Elemental mapping (a) and quantification (b) of elemental composition of MSs via EDS analysis. The white arrow in BSG indicates regions with higher Na and Al contents and lower Si and K contents. ***$p < 0.001$. Error bars represent S.E.M. Scale bar—300 $\mu$m.

**Table 4. Measured Elemental Composition (mole % ± S.E.M.) of MSs Using EDS Analysis**

| glass | $P_2O_5$ | CaO | MgO | $Na_2O$ | $Fe_2O_3$ |
|---|---|---|---|---|---|
| P45-B | 44.7 ± 0.1 | 16.7 ± 0.1 | 26.2 ± 0.2 | 8.6 ± 0.1 | 3.8 ± 0.1 |
| P40-B | 43.3 ± 0.1 | 14.8 ± 0.1 | 23.6 ± 0.8 | 18.3 ± 0.1 | 0 |
| P40-P | 39.5 ± 0.1 | 22.8 ± 0.3 | 21.2 ± 0.5 | 16.7 ± 0.1 | 0 |

mean sphericity of 0.8. SEM images also showed a large number of small particulates (<10 $\mu$m in size) attached on the surface of BSG, consistent with the MAL offset distribution curve. The porous MS P40-P had more particulates present on its surface, again consistent with the offset distribution curve. The pore windows measured on P40-P had a mean MAL of 4.1 ± 0.1 $\mu$m ($n$ = 7023 pores from ~30 MS in 23 SEM images, Figure 1d). To further investigate the internal pore structure of these particles, Cryo-FIB SEM was performed. The results (Supporting Information S3, Figure S6) showed the presence of interconnected pores with some interconnecting tunnels of <5 $\mu$m in size.

All the other physical measurements and degradation observations of MS are tabulated in Table 3 and shown in Supporting Information S3, Figure S7. The BET measurements for all the bulk MS showed a surface area of below 0.1 $m^2/g$. As expected, the surface area for P40-P was significantly higher, measured at 0.877 ± 0.268 $m^2/g$ (ranging from 0.627 to 1.144 $m^2/g$) and was 10 times higher than that of all bulk MSs used in this study. In addition, approximately twice as much closed porosity was calculated in the porous MS P40-P at 11.5% compared to other MSs. Mean tapped densities of the bulk MS ranged between 1.13 and 1.31 $g/cm^3$, approximately twice that of the porous MS P40-P. When these values were normalized to their respective closed porosities, the normalized tapped density for bulk MS ranged between 1.20 and 1.41 $g/cm^3$, which was again nearly twice as much of porous MS P40-P.

*3.1.2. Elemental Composition of MSs.* The EDS spectral analysis (see Figure 2a,b and Table 4) showed that BSG had a chemical composition of $B_2O_3$-$SiO_2$-$Na_2O$-$Al_2O_3$-CaO at 9.5-82.0-5.5-2.0-1.0%, with a measurement error of 2%. The composition measurements for PBG MSs (Table 4) generally followed the nominal composition (Table 1), although there were statistically significant differences in all oxide compositions observed relating to the glass processing route. In particular, a relatively high value of $P_2O_5$ at 43.3% rather than 40% was observed for P40-B (Figure 2b). Of further interest is the difference between the Ca and P contents in P40-B and P40-P due to the additional processing step used to manufacture the porous particles. This appeared to be spatially sensitive as the EDS spectrum and mapping analysis (Supporting Information S3, Figure S8a,b) at higher magnification clearly showed a higher amount of Ca and lower amounts of P, Mg, and Na near the edges of some of the pores in P40-P. Higher amounts of Ca in P40-P were also validated by XPS analysis (Supporting Information S3, Figure S12a).

*3.1.3. Morphological Changes on MSs during Incubation in Water and Culture Medium.* To study the effect of hydration, a preliminary experiment was performed where MSs were incubated in ultrapure water for 1 day, and then, SEM examination was performed (Supporting Information S3, Figure S9). While the BSG remained unaffected by exposure to water, the effect of hydration was clearly visible on PBG MSs. P45-B and P40-B had circular cracks with crater-like perforations on their surface. However, P40-P had crater-like perforations in addition to delaminating pore edges.

To study these morphological changes in more detail, MSs were incubated in SC medium for 6 weeks. Results again showed cracks and delamination on both bulk and porous PBG MSs; however, there were differences in the appearance of cracks developed on different MSs (Figure 3). For bulk MSs P45-B and P40-B (Figure 3a–g), small-lined features


https://doi.org/10.1021/acsabm.1c00120
ACS Appl. Bio Mater. 2021, 4, 5987–6004

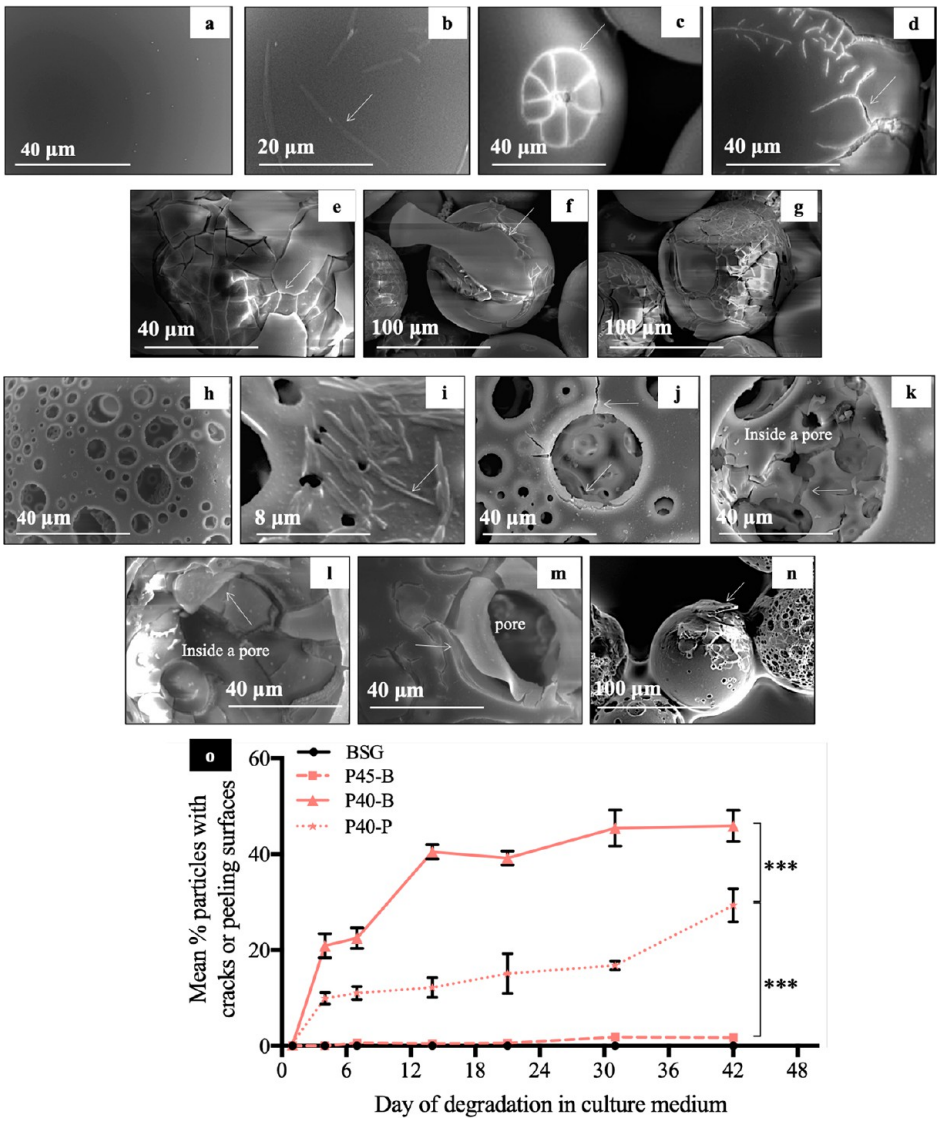


**Figure 3.** Progression of surface damage on bulk and porous PBG MSs as a result of degradation in culture medium over 42 days. In the case of bulk PBG MSs (a–g), cracks and delaminating surfaces were visible. In the case of P40-P (h–n), the cracks and delaminating surfaces (arrows) developed around and inside the pores. (o) Quantification of degradation of MSs in culture medium. Highest surface damage was on P40-B (46%) and then P40-P (29%), followed by P45-B (2%) and BSG (0%) after 42 days of degradation in medium; $n = 5$ fields of view per MS type per time point. ***$p < 0.001$. Error bars represent S.E.M.

with swelling were visible at early time points, and then smaller cracks also started to appear. The cracks were much larger in size at later time points and often coupled with delamination of the glass surface. The cracks were not only limited to the top surface of the MS but also developed underneath the delamination surface, leading to total disintegration of the MS surface. In the case of the porous MS, P40-P (Figure 3h–n), cracks were observed near the pore edges, on the glass surface, and also in the internal pore cavities (Figure 3k). Delamination was visible in the vicinity of these cracks. The cracks and delaminating surfaces appeared at a much faster rate on P40-B and P40-P compared to P45-B (Figure 3o).

To confirm that the occurrence of surface damage on PBG MSs was not due to dehydration during sample preparation for SEM, P40-P was analyzed with ESEM in ultrapure water. The results (Supporting Information S3, Figure S10) showed that even after a short period of time (1 h 45 min), these particles incurred cracks on their surface, in line with the abovementioned two experiments.

**3.2. Cytocompatibility.** The potential of PBG MSs for bone regenerative applications was explored via several cell-based experiments.

*3.2.1. Cell Attachment on MSs.* For the assessment of cell attachment, MSCs were seeded at 2500, 5000, and 10,000 cells/cm$^2$ (5000, 10,000, and 20,000 cells in 200 $\mu$L per well), and after 24 h, cell metabolic activity and DNA measurements were performed. The results (Figure 4a) showed a general decreasing trend in cell metabolic activities, where BSG > P45-B > P40-B > P40-P ($p < 0.05$) for 2500 and 5000 cells/cm$^2$ densities. The DNA content measurements (Figure 4b) showed significantly lower values in P40-P compared to other conditions ($p < 0.05$) at 5000 and 10,000 cells/cm$^2$.

*3.2.2. Cell Viability on MSs.* To explore the viability of MSCs seeded at 2500 cells/cm$^2$ (5000 cells in 200 $\mu$L per well), FDA/PI staining was performed on day 1 and 4 of


https://doi.org/10.1021/acsabm.1c00120
ACS Appl. Bio Mater. 2021, 4, 5987–6004

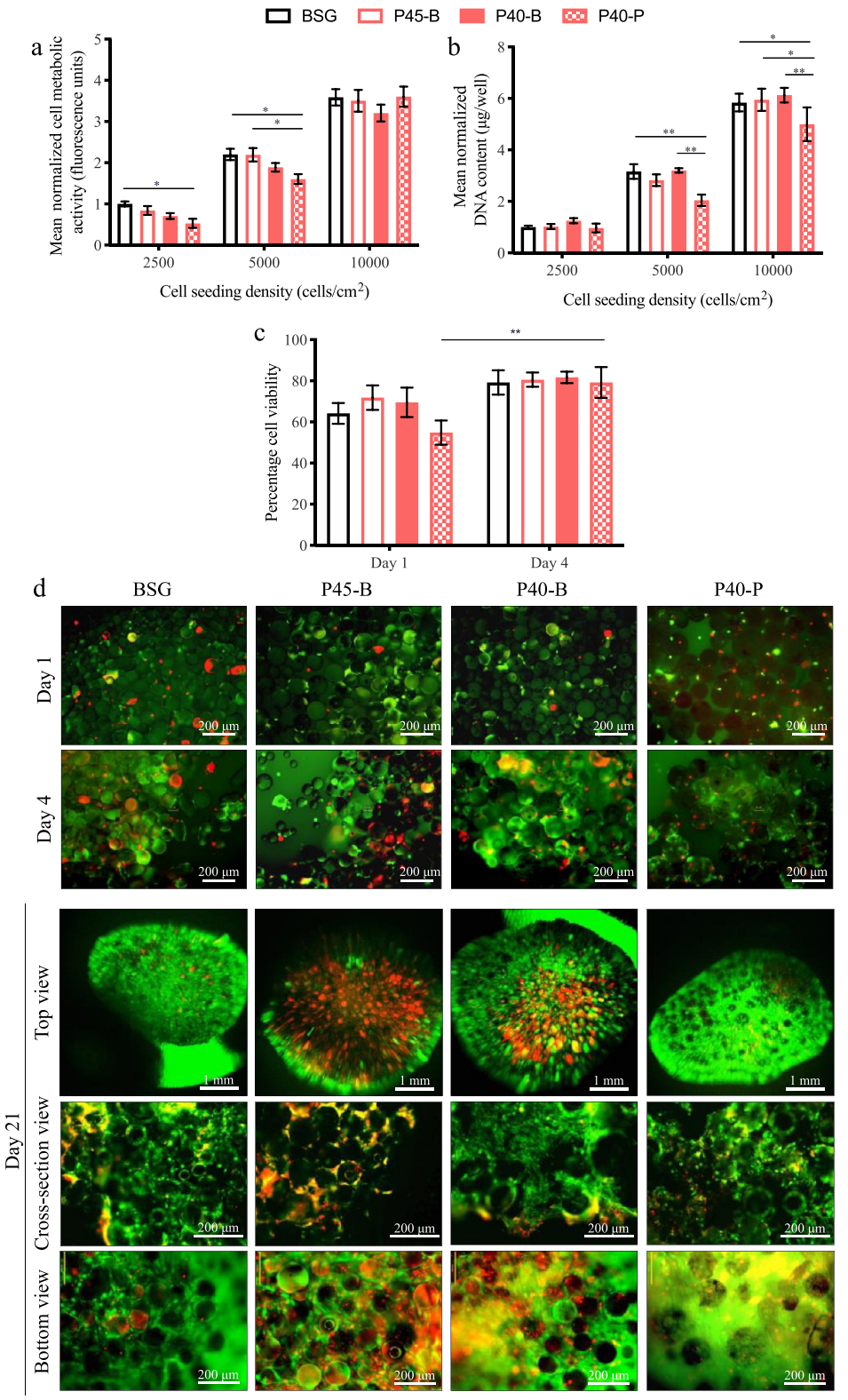


**Figure 4.** Viability of human MSCs seeded on MSs. Cell metabolic activity in panel (a) and DNA content assays in panel (b) were performed after 1 day ($n = 6$). Cell viability assessed on day 1, 4, and 21 of culture ($n \geq 3$) is shown in panel (c). Representative images of live (green) and dead (red) MSCs on day 1 and day 4, with top, bottom, and cross-sectional views of different 3D aggregates at day 21 of culture are shown in panel (d). *$p < 0.05$ and **$p < 0.01$. Error bars represent S.E.M.

culture. The results (Figure 4c,d) showed significantly lower numbers of viable cells on P40-P compared to all other bulk MS conditions on day 1 of culture ($p < 0.05$). However, by day 4, this deficit was no longer present, and the cells on P40-P showed a similar viability to that of other conditions. On day 21 of culture, cell viability was assessed from three regions of 3D aggregates: top (region of the aggregate facing the well plate lid), bottom (region of the agglomerate facing the



https://doi.org/10.1021/acsabm.1c00120
ACS Appl. Bio Mater. 2021, 4, 5987−6004

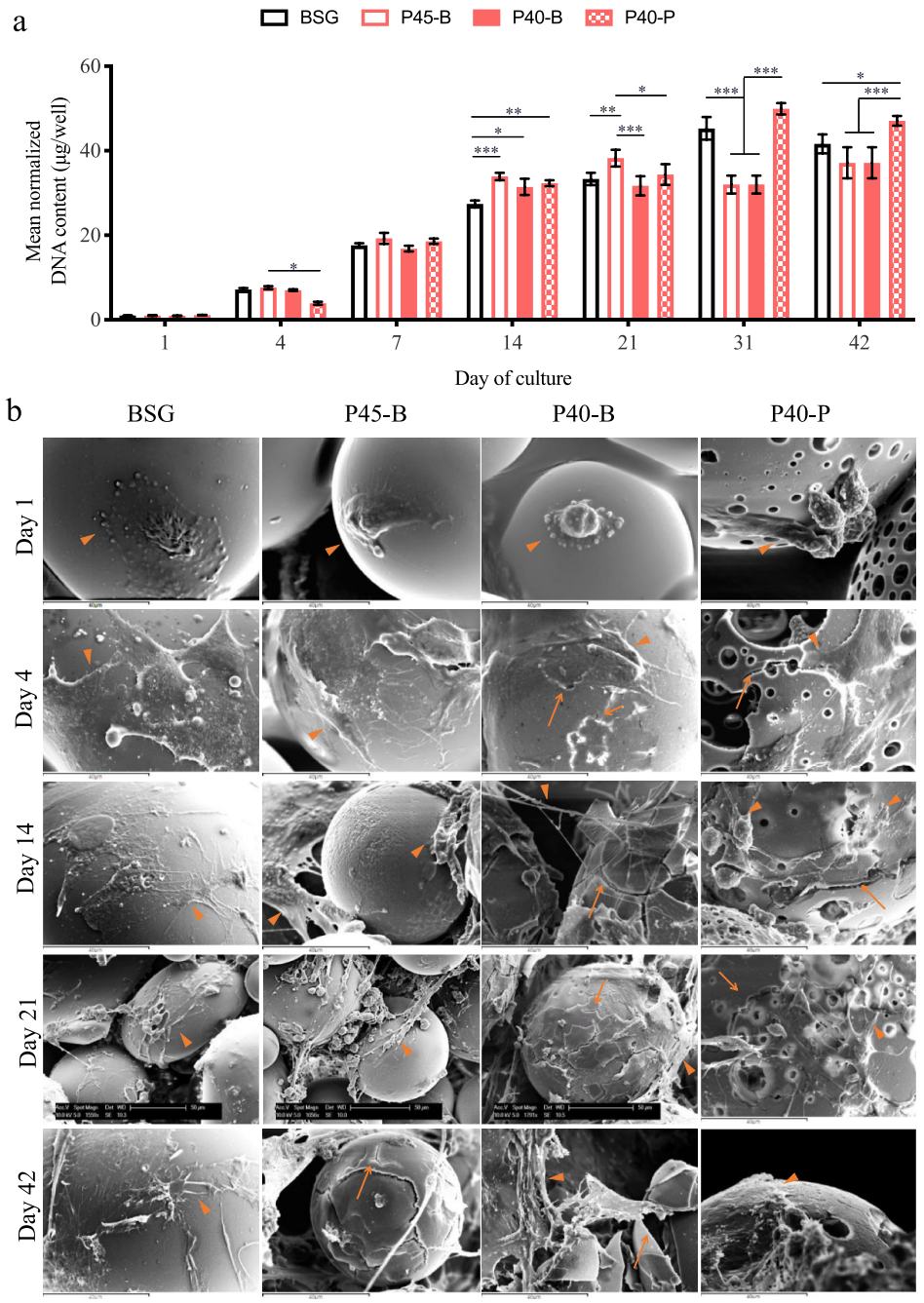


**Figure 5.** Human MSC growth on MS. (a) DNA content measurements and (b) SEM images of cells growing over 42 days of culture. *$p < 0.05$, **$p < 0.01$, and ***$p < 0.001$. Cells and surface damage on MSs are indicated by orange arrowheads and arrows, respectively. Scale bars—40 $\mu$m.

bottom of the well), and cross-section (internal region of the 3D aggregate observed after cryo-sectioning). The results clearly showed more cell death in P45-B as compared to all other MS conditions, in all three regions, suggesting a negative effect of the P45 chemical formulation on MSCs.

*3.2.3. Cell Growth on MSs.* To study cell growth directly on different MSs, GFP-labeled MSCs were seeded at 2500 cells/cm$^2$ (5000 cells in 200 $\mu$L per well). Comparison of bulk MSs showed that by day 31, there was significantly higher DNA content on BSG than on P45-B and P40-B ($p < 0.05$, Figure 5a). However, by day 42, no significant differences were observed among these conditions. Comparison of P40-B and P40-P suggested that porosity may have negatively affected MSC growth on day 4 of culture ($p < 0.05$), but beyond this time point, cell growth increased steadily, showing the highest mean DNA content by day 31 and day 42 ($p < 0.05$).

*3.2.4. Human MSC Morphology on MSs.* To explore MSC morphology on different MSs, SEM was carried out on day 1, 4, 14, 21, and 42 of culture after cell seeding at 2500 cells/cm$^2$ (5000 cells in 200 $\mu$L per well) (Figure 5b). Cells seeded on bulk MSs displayed a flat morphology on day 1 and day 4, but cells seeded on the porous P40-P were observed to have a round morphology, suggesting poorer cell attachment. During extended culture periods, more rounded cells started to appear primarily on P45-B and less so on BSG. However, in the case of P40-B and P40-P, cells were seen to interact with cracks and delaminating glass surfaces from day 4 onward. Cells were



https://doi.org/10.1021/acsabm.1c00120
ACS Appl. Bio Mater. 2021, 4, 5987−6004

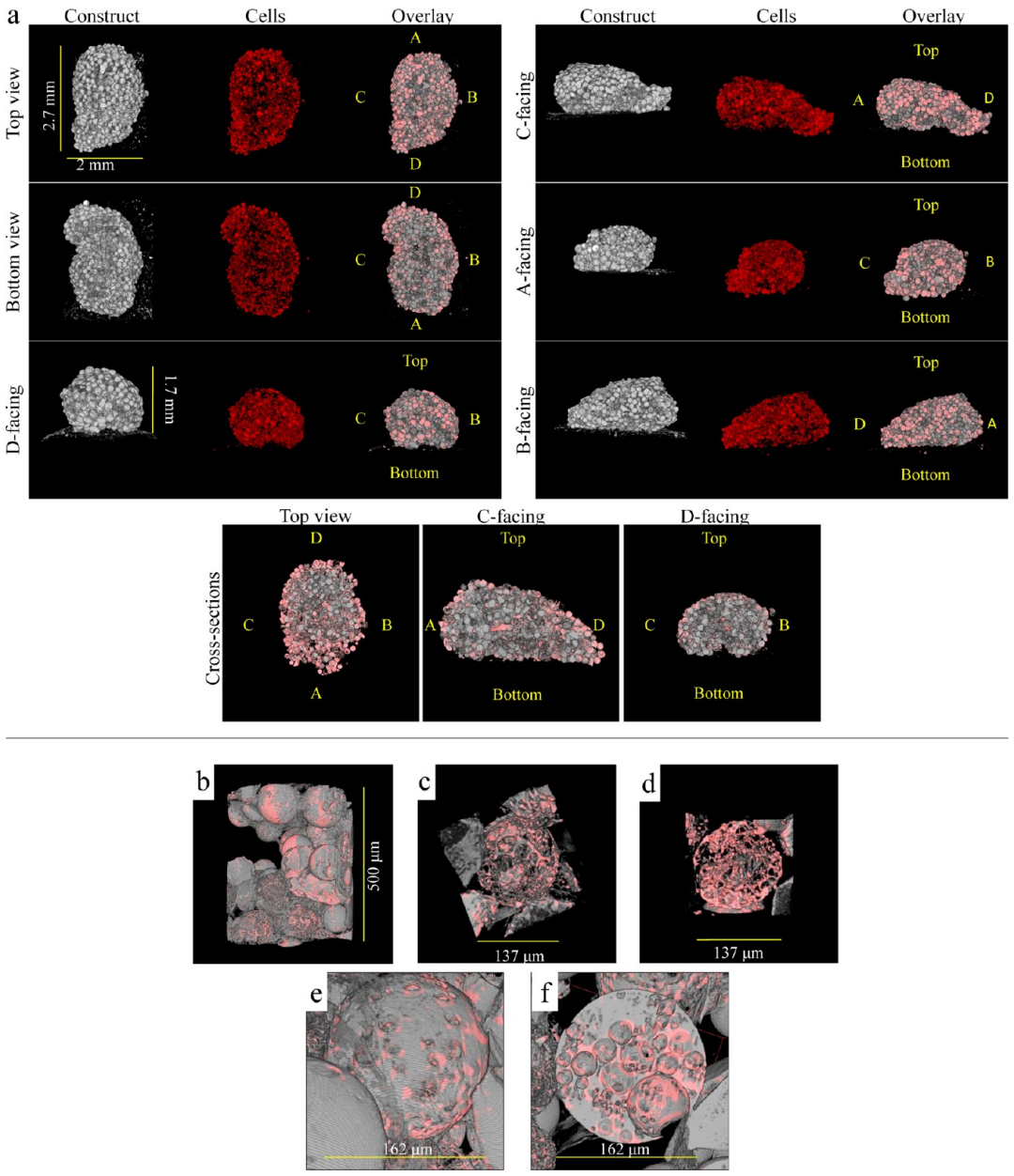


**Figure 6.** Micro-CT of cell-P40-P aggregates after 7 days of culture. (a) 3D tomography of the construct (P40-P), cells (red), and overlay (construct + cells) from all the faces of the aggregate has been shown. The "top" faces the top of the well plate, and the "bottom" faces the bottom of the well. A, B, C, and D are the four lateral faces of the aggregate. There were more cells present in the top face than in the bottom face, while the lateral faces showed similar cell distribution. Cross-sectional views from the top, C, and D faces showed more cells on the outer edges than on the inside of the aggregate. (b–f) Cell colonization inside P40-P. (b) Higher resolution scan of the cells + P40-P aggregates shown in panel (a). The cells seem to be unevenly distributed on P40-P. (c) Highly porous glass MSs had cells present on the outer surface of the MS and on the inside as shown in panel (d) via a cross-section. On the other hand, there were relatively less cells present on the outer surface of a porous MS, which had lesser pores on its surface (e) and a cross-sectional view (f) also showed the same.

observed to grow over and around the pores. Micro-CT scans were performed to further assess the penetration of cells inside the porous MS P40-P (Figure 6a), through 3D reconstructions. After 7 days of culture, there was a higher density of cells on the region facing the top of the well plate compared to the region facing the bottom of the well plate. Cross-sectional views showed more cells present on the outer edges of the aggregates relative to the internal regions. Visual inspection also confirmed that MSs presenting larger pores contained more cells (Figure 6b–f).

*3.2.5. Cytotoxicity Assessment of MSs.* Three different cytotoxicity evaluations were performed, as described in Section 2.7.3. In the transwell plate (material-to-medium ratio was 100 mg/1 mL), cells exposed to P40-B- and P40-P-eluted media over 3 days showed higher metabolic activity compared to those under other conditions ($p < 0.05$) (Figure 7a). Particulates were seen floating in the P40-B and P40-P-eluted media (faster degrading MSs), which was not observed in other conditions (Figure 7b). When these particulates were analyzed using EDS (Figure 7c), their elemental composition



https://doi.org/10.1021/acsabm.1c00120
ACS Appl. Bio Mater. 2021, 4, 5987–6004

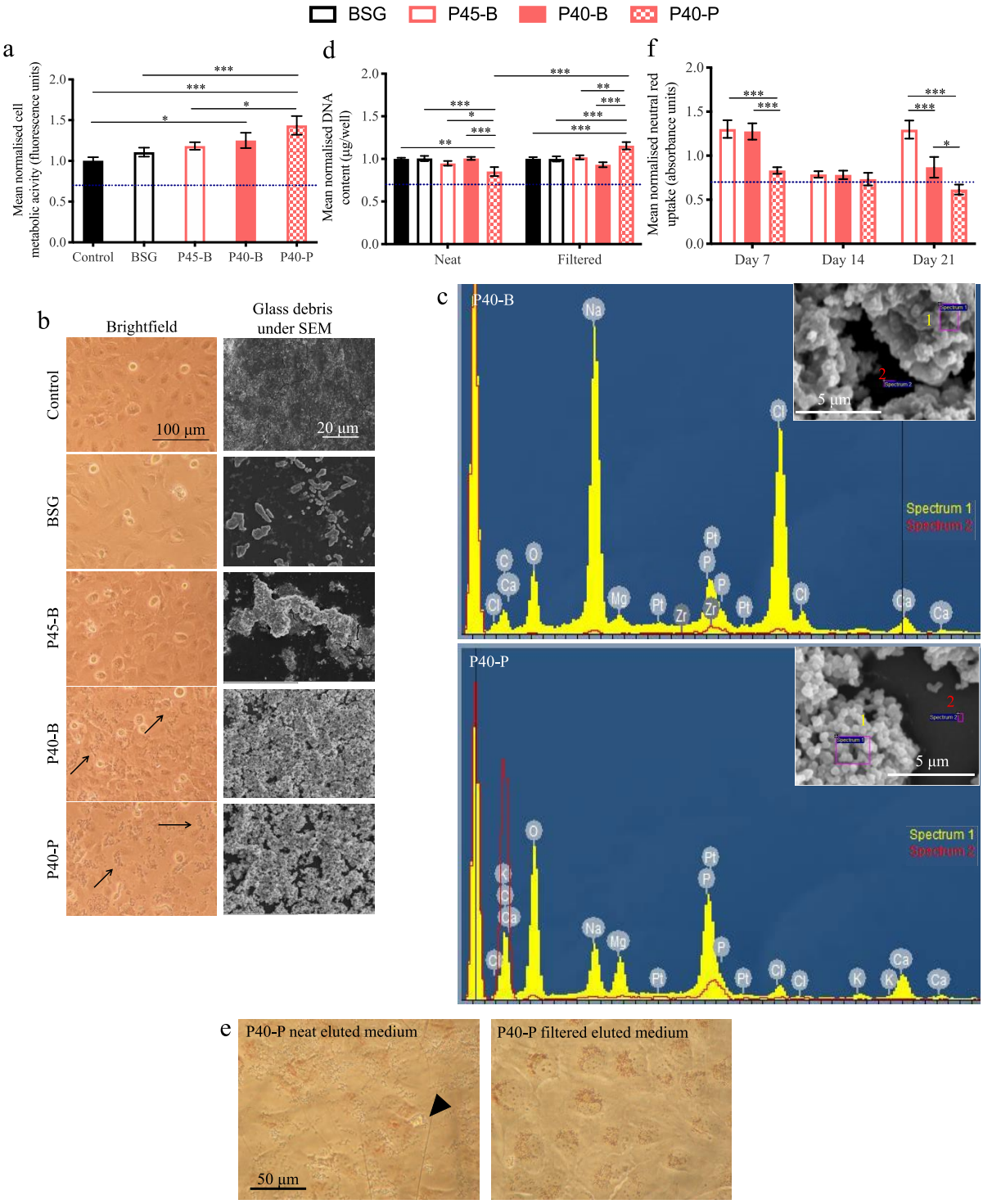


**Figure 7.** Indirect-contact cytotoxicity evaluation for the glass MS. (a) Human MSC metabolic activity over 3 days of exposure to MS-eluted media via transwell, $n = 3$. (b) Bright field images of cells taken on day 3 of exposure. Notice the presence of particulates floating in the case of P40-B and P40-P (arrows). These particulates were collected and analyzed used SEM. (c) EDS analysis of particulates showed that they were released from P40 glass, as they had similar elemental composition as the MS composition. (d) Extract tests of MS after 7 day of elution in medium. The day 7 eluted medium was either used as neat or filtered using a 0.4 $\mu$m filter and exposed to MSCs for 24 h and evaluated using DNA assay. (e) Neutral Red dye uptake by MSCs exposed to P40-P-eluted medium. Arrowheads indicate glass particulates in the vicinity of the cells in neat extracts but not in filtered extracts. For panels (a,d), all measurements were normalized to the respective control (no MS, medium-only). (f) Cytotoxicity of spent medium removed from the MSC-loaded MS on day 7, 14, and 21 of culture. (-----) indicates 70% viability compared to BSG-spent medium in panel (f) and control (no MS) in panels (a,d). *$p < 0.05$, **$p < 0.01$, and ***$p < 0.001$. Error bars represent S.E.M.

was similar to that of P40 glass, indicating that these debris were released from the MS.

To determine whether these particulates affected cell proliferation, MSs were eluted in culture medium for 7 days



https://doi.org/10.1021/acsabm.1c00120
ACS Appl. Bio Mater. 2021, 4, 5987−6004

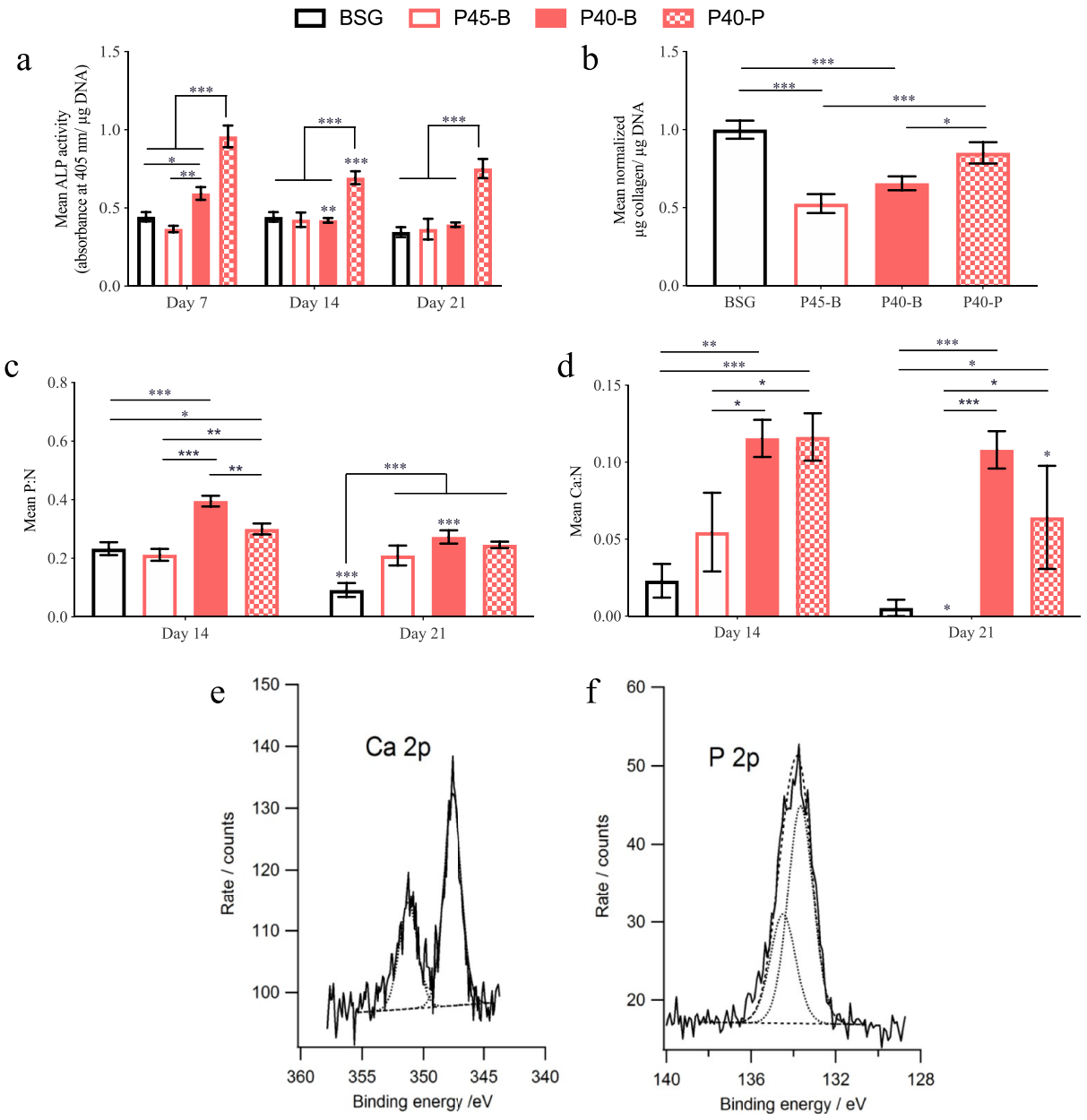


**Figure 8.** Effect of MSs on the osteogenic differentiation of MSCs. (a) ALP activity of MSCs grown on MSs over 21 days. (b) Collagen production by MSCs grown on MSs on day 21. (c) P/N and (d) Ca/N ratio in the ECM of cells after 14 and 21 days of culture. XPS high-resolution spectra of (e) Ca 2p and (f) P 2p in the P40-B + cell sample on day 21 showing the presence of a precursor bone-like material. *$p$ < 0.05, **$p$ < 0.01, and ***$p$ < 0.001, relative to previous time point unless otherwise mentioned. Error bars represent S.E.M.

(material-to-medium ratio was 100 mg/1 mL) in the second cytotoxicity evaluation, and the eluted medium with or without filtration was added to pre-seeded MSCs. After 24 h of exposure, DNA content measurements showed significantly more cells present in filtered medium compared to neat medium in the case of P40-P-eluted medium (Figure 7d). However, this was not observed for any other MS types. Viability staining with Neutral Red (Figure 7e) indicated that the cells were viable under all conditions; however, there were glass fragments/particulates around the cells in neat P40-P-eluted medium but not in the filtered P40-P-eluted medium.

To assess whether the presence of cells seeded onto the glass material might reduce the release of the glass particulates, a final set of cytotoxicity experiments was performed where MSCs were loaded onto MSs and grown for 21 days as in direct-contact experiments (material-to-medium ratio was approximately 20 mg/1 mL for bulk MSs and 10 mg/1 mL for the porous MS). The spent medium collected on day 7, 14, and 21 was transferred (neat) to a new well plate pre-seeded with MSCs. The results (Figure 7f) showed that the lowest cell viability was detected in P40-P spent medium collected on day 7 and 21 ($p$ < 0.05). In addition, floating glass particulates/fragments were also seen in the spent medium collected from P40-B and P40-P, indicating that despite the presence of cells on their surface, glass debris were released from these MSs, which may have a cytotoxic effect on other MSCs (Supporting Information S3, Figure S11).

Altogether, these cytotoxicity results suggested that MSs released glass particulates whether or not they were seeded



https://doi.org/10.1021/acsabm.1c00120
ACS Appl. Bio Mater. 2021, 4, 5987−6004

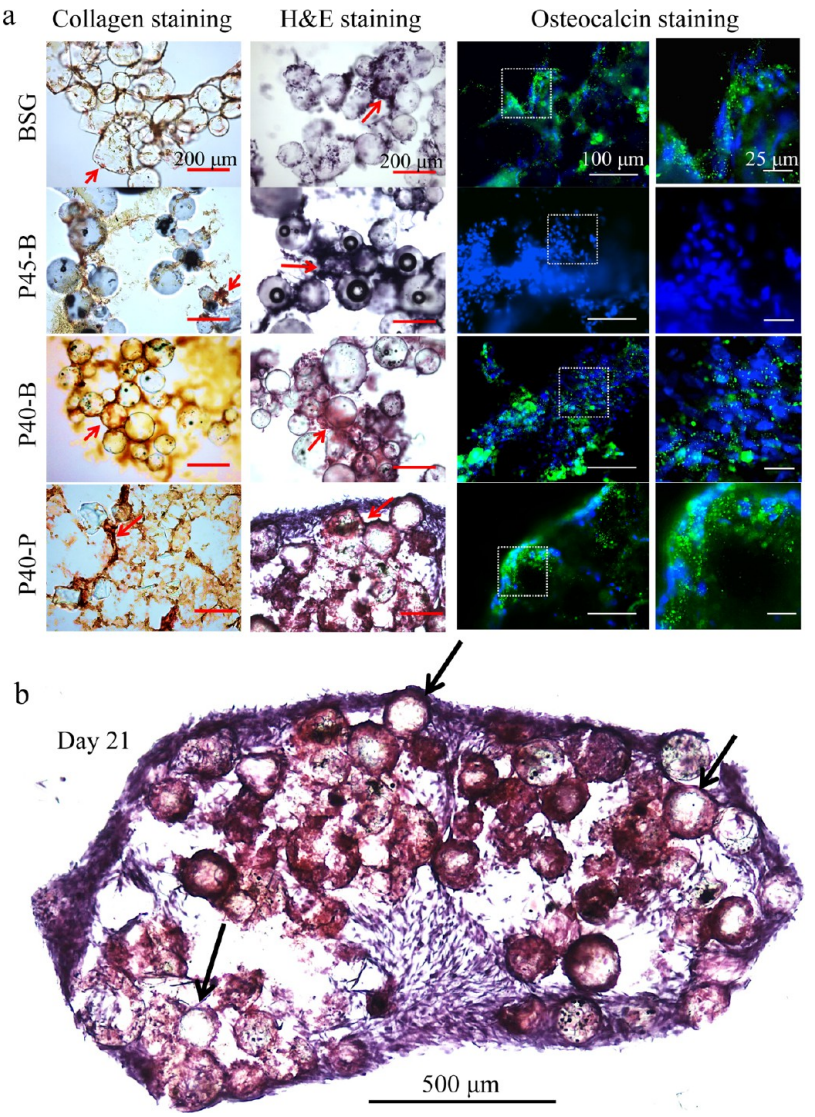


**Figure 9.** (a) Qualitative analysis of collagen production, ECM formation, and osteocalcin expression by MSCs on different glass MSs using Sirius Red staining, H&E staining, and immunostaining, respectively after 21 of culture. Arrows indicate collagen- or ECM-rich regions. For osteocalcin staining, the green signal represents positive staining and the blue signal represents DAPI staining the nucleus. Lined boxes in the third column are the regions magnified in the last column for osteocalcin staining. (b) H&E-stained section of P40-P + cells after 21 days of culture. Arrows indicate MSs with staining restricted to outer regions.

with cells, and these particulates may negatively affect MSC growth.

*3.2.6. Effect of MSs on Osteogenic Differentiation of MSCs.* To investigate the osteogenic response to the MS, MSCs were seeded at 10,000 cells/cm$^2$ (20,000 cells in 200 $\mu$L per well) in SC medium on the different MS types, and ALP activity was assessed on day 7, 14, and 21 of culture. The results (Figure 8a) showed highest ALP activity for P40-P at all time points ($p < 0.001$) and significantly higher ALP activity for P40-B compared to BSG ($p < 0.05$) and P45-B ($p < 0.01$) on day 7 only. These results strongly suggested that faster degrading P40-B had an osteogenic effect, and the introduction of porosity potentiated this ability further.

Analysis of collagen production, a late osteogenic differentiation marker, showed a higher collagen signal for cells on P40-P compared to that on P45-B and P40-B ($p < 0.05$) (Figure 8b). These results highlighted the positive effect of porosity on collagen production by MSCs. After 21 days of culture, Sirius Red-, H&E-, and anti-osteocalcin-stained cryosections of 3D aggregates also showed higher collagen, ECM, and osteocalcin signals in both P40 MS formulations relative to BSG or P45-B and the absence of osteocalcin in P45-B (Figure 9a). The low-magnification view of H&E-stained P40-P + cell aggregate sections after 21 days of culture highlighted preferential positive eosin staining in the regions in and around pores (Figure 9b).

To study the Ca and P found in the ECM of cells present on the top face of different 3D aggregates, XPS analysis was performed on days 14 and 21 of culture (Supporting Information S3, Figure S12, Supporting Information S1, Table S3). The results (Figure 8c,d) showed higher mean P/N and mean Ca/N in P40-B and P40-P relative to P45-B and BSG on both time points, indicating a positive effect of P40 glass formulation on P and Ca deposition by cells. For the high-resolution Ca 2p and P 2p spectra, more detailed modeling was applied to examine the chemical states of Ca and P. The P 2p peak was at 133.2 eV with a fwhm of 1.2 eV, at the listed position and peak width for $(PO_4)^{3-}$. This applied


https://doi.org/10.1021/acsabm.1c00120
ACS Appl. Bio Mater. 2021, 4, 5987−6004

to all the samples at day 21. The Ca $2p_{3/2}$ peak was at 347.6 eV, consistent with $CaH(PO_4)$,[45] which confirmed the formation of a bone-like matrix in these samples. An example peak fit for Ca 2p and P 2p of the P40-B + cell sample is shown in Figure 8e,f.

## 4. DISCUSSION

Previously, a number of studies have explored the cytocompatibility of PBGs used in the form of fibers, discs, and microspheres for culture experiments lasting up to 3 weeks. Here, different phosphate-based glass formulations ($P45:45P_2O_5$-16CaO-24MgO-$11Na_2O$-$4Fe_2O_3$, mol %, and $P40:40P_2O_5$-16CaO-24MgO-$20Na_2O$, mol %) were investigated, with and without porous morphology, with a cytocompatibility study extended to 6 weeks in culture. This study was designed to compare a slow-degrading (P45-B) and relatively faster degrading (P40-B, P40-P) MS systems, with or without pores, to compare bone marrow-derived human MSC responses as a relevant cell model for bone repair and reinforcement applications. The results revealed that it is the combined effect of morphological changes occurring on the surface of glass and degradation products released from the glass material as a result of degradation that determines the stem cell response.

Overall, the different bulk MS types had similar particle size distribution, while the porous P40-P differed significantly, due to the release of $CO_2$ gas from the porogen during the flame spheroidization process, causing the particles to expand in size and leaving a porogen residue (calcium-based) deposited near the edges of the pores. The surface area measurements were less than 0.1 $m^2/g$ for all bulk MS, in line with surface area measurements for commercially available non-porous MSs such as Biosilon (160−300 $\mu$m, 0.030 $m^2/g$), Hillex (150−210 $\mu$m, 0.035 $m^2/g$), and the glass MS by SoloHill, USA (15−210 $\mu$m, 0.038 $m^2/g$). Moreover, P40-P demonstrated a 10 times higher surface area due to the effect of porosity, and these values are in accordance with the previously reported surface area measurements for non-porous and porous PBG MS[16] and also comparable to those of the commercially available cellulose-based porous MS Cytopore (200−280 $\mu$m diameter, 30 $\mu$m mean pore windows, and 1.100 $m^2/g$ surface area) by Amersham Biosciences, Sweden.

Both P40-B and P40-P were more prone to hydration, and there were visible signs of surface damage as early as day 1 or day 4 of culture, which became significant over a period of 42 days. The cracks and delaminating surfaces may have affected cell attachment and proliferation. Moreover, some of the ECM deposited by the cells may have been lost with the delaminating glass surfaces.[17] Cytotoxicity evaluations confirmed that P40 MS released glass particulates into the culture medium, and their removal via filtration could enhance cell proliferation. Some previous studies have shown that glass particulates less than 10 $\mu$m wide can be internalized by cells[46] where they may interact with different organelles based on their chemistry, size, and shape and affect cell viability.[47] Further analysis such as transmission electron microscopy needs to be performed to study the interaction between PBG glass debris and cells.

Surface damage on glass implants is a commonly occurring phenomenon, and it has been associated with faster degrading glasses in all forms such as fibers,[48] MSs,[49] and discs.[17] PBGs are especially known to swell up in aqueous solutions, leading to perforations.[48] Manufacturing MSs used in this study involved rapid cooling after the spheroidization step, which may have led to the development of stresses in the MS glass structure. In the case of bulk MSs, the core may have cooled at a slower rate compared to the outer regions, resulting in residual compressive stress on the surface. Then, when the sphere was transferred into aqueous medium, the swelling may have caused regions to crack as it expanded. In the case of P40-P, the low-volume areas such as extremities of glass struts may have cooled quickly, leading to crack formation and subsequent peeling of surfaces. Annealing at higher temperatures of 450 °C has been shown to delay degradation and surface peeling of bioresorbable glass fibers.[48] Similar observations were also reported by Parsons et al.[50] after annealing PBG fibers. In future, it may be worth exploring different formulations of PBGs and annealing temperatures to minimize glass delamination and particulate release from glass MSs.

The accelerated ion release due to glass degradation is also suggested to affect cell fate. Gough et al.[51] showed that 50% of human osteoblasts cultured in neat extracts of porous bioactive glass scaffolds (60 mol % $SiO_2$, 36 mol % CaO, and 4 mol % $P_2O_5$) underwent apoptosis-like cell death after 24 h of culture, possibly due to the excessive release of calcium and silica ions. Excess $PO_4^{3-}$ in the blood has been associated with ectopic calcification in soft tissues[52] and apoptosis in endothelial cells.[53] Previously, Hossain et al.[16] investigated the $Ca^{2+}$ and $PO_4^{3-}$ release rates in DMEM (10 mg/mL material to medium ratio) and found them to be in the range of 45 ± 1 and 34 ± 2 ppm/day for the solid non-porous P40 MS (108 ± 10 $\mu$m wide) and 47 ± 3 and 49 ± 3 ppm/day for the porous P40 MS (125−200 $\mu$m wide size range). Using these values and the fact that the material-to-culture medium ratio in direct-contact cell experiments in the present study was approximately 20 mg/1 mL for P40-B and 10 mg/1 mL for P40-P (as the MSs were normalized to the surface area for cell culture), the $Ca^{2+}$ and $PO_4^{3-}$ release rates for these MS can be calculated to be 90 and 68 ppm/day for P40-B and 47 and 49 ppm/day for P40-P, respectively. As the culture medium changes in these cell experiments were performed every 2−3 days, this may have led to accumulation of 180−270 ppm $Ca^{2+}$ and 136−204 ppm $PO_4^{3-}$ in P40-B-exposed medium and 94−141 ppm $Ca^{2+}$ and 98−147 ppm $PO_4^{3-}$ in P40-P exposed medium. Liu et al.[54] suggested that optimal doses of extracellular $Ca^{2+}$ and $PO_4^{3-}$ for MSC growth and differentiation are 72 and 8.5 ppm, respectively, and any increase or decrease in these values would be detrimental for the cells. Moreover, higher than 8.5 ppm $PO_4^{3-}$ led to significant cell apoptosis. Hence, high extracellular $Ca^{2+}$ and $PO_4^{3-}$ concentration in P40-B- or P40-P-exposed culture media may have affected MSC proliferation and caused cytotoxicity.

Degradation profiles for P45 and P40 glass discs (9 mm diameter, 4 mm thick) have also been reported elsewhere.[15] The study showed nearly 0.8% and 4% of mass loss, respectively, after 42 days of degradation in PBS. The five times slower mass loss of P45 glass may also be correlated to the reduced surface peeling off effect observed in the case of P45-B than in P40-B in the present study. Thus, using these values, approximate $Ca^{2+}$ and $PO_4^{3-}$ release rates of P45-B can be calculated as 9 and 6.8 ppm/day, respectively, leading to accumulation of 18−27 ppm $Ca^{2+}$ and 13.6−20.4 ppm $PO_4^{3-}$ in P45-B-exposed medium before medium changes were performed in direct-contact cell experiments. In this case, high


https://doi.org/10.1021/acsabm.1c00120
ACS Appl. Bio Mater. 2021, 4, 5987−6004

extracellular $PO_4^{3-}$ may have been a source of cytotoxicity. Some $Ca^{2+}$ and $PO_4^{3-}$ may have also been deposited in the ECM over time and could have contributed to the levels measured via XPS.

In addition to degradation products, the presence of pores on the P40-P may have also affected MSC fate. It is well known that the presence of grooves and pits on 2D surfaces can alter cellular responses such as adhesion, migration, and osteogenic differentiation.[55] For instance, Park et al.[56] reported that MSCs actively avoided concave surfaces (200−300 $\mu$m wide and 50−150 $\mu$m deep) made from poly(dimethylsiloxane) during culture. Fischer et al.[57] also reported reduced cell proliferation on hydroxyapatite MSs (212−300 $\mu$m diameter) between day 4 and day 7. At the molecular level, myosin II mini-filaments bind together to form 300 nm rods that are stiff in nature, and when stimulated via the Rho/ROCK pathway, these rods orient themselves along the axis of the least curvature for full head engagement with the underlying surface, which translates into cell attachment.[58] This allows the cell to adapt to the underlying material surface curvature. In the case of high-curvature regions in P40-P such as pore surfaces and sharp pore edges, the engagement of rod heads may not be sufficient and may have resulted in reduced MSC attachment and survival on P40-P.[59]

The cell growth experiments consistently showed that despite the 10-fold higher surface area of P40-P, there was only 1.6 times more DNA content measured for cells grown on it relative to cells grown on P40-B at a later time point. This could be due to a technical limitation of using sonication to recover DNA, which may not be as efficient for cells in pores (P40-P) as compared to cells on the surface (P40-B). It may also be due to the vast majority of pore windows less than 5 $\mu$m wide that could have limited cell penetration during the culture period, a possibility supported by micro-CT 3D tomography (Figure 5). Similar observations have also been reported by Berry et al.,[60] who grew fibroblasts on 2D pitted surfaces and found that cells migrated in pits with 25 $\mu$m diameters and not in 7 or 15 $\mu$m wide pits.

P40-B and P40-P were found to be most suitable for osteogenic differentiation of MSCs. Intracellular $Ca^{2+}$ can enhance glutamate secretion inside cells,[61] which may be responsible for promoting an osteogenic fate.[62] Therefore, the $Ca^{2+}$ released in medium as a result of P40 glass degradation may have favored early osteogenesis in MSCs. These results are in line with a previous study where MG-63 cells seeded on P40 glass discs had higher ALP activity compared to the cells on P45-glass discs or tissue culture plastic.[15] Another study suggested that convex surfaces may induce higher ALP activity,[38] which may explain the enhanced ALP activity observed in MSCs seeded on porous P40 MSs. This also fits with Barrias et al.[63] who reported that rat bone marrow stromal cells expressed higher ALP activity when cultured on porous hydroxyapatite MSs (607 ± 30 $\mu$m diameter, <5 $\mu$m pores) compared to those on smooth plastic MSs (205 ± 120 $\mu$m diameter).

A number of in vivo studies have suggested that bone formation occurs preferentially in concavities of 3D scaffolds. For example, Ripamonti and co-workers showed extensive bone formation in concavities of highly crystalline porous hydroxyapatite implanted in adult baboon muscles for a period of 1−9 months.[6] More recently, Gao et al.[64] reported preferential bone formation in porous regions of $\beta$-tricalcium phosphate granule scaffolds after 4−12 weeks of implantation in rabbit femurs. Similar observations have been reported in vitro. For example, micro-pits of 20−40 $\mu$m diameter on 2D surfaces led to significantly more nodule formation by human osteoblastic cells compared to planar surfaces after 21 days of culture without osteogenic factors.[65] Additionally, collagen deposition has been shown to occur preferentially in the tissue−pore interface of the concavities.[66] Altogether, these studies strongly indicate that porous regions of P40-P may be able to induce osteogenic differentiation over longer culture periods.

Finally, results produced here suggest that P45-B materials were least favorable for bone matrix formation by MSCs. While the presence of Fe−O−P bonds in P45 glass may have made it more resistant to hydration,[67] it may have also made the glass surface more hydrophobic, ultimately contributing to less-efficient cell migration and survival on P45-B. A publication reported an increase from 13 to 26° in contact angle measurements as the Fe content in the $P_2O_5$-CaO-$Na_2O$ glass system increased from 0 to 5% (mole %) for flat-surfaced conventional melt cooled glass.[68] The curved morphology of P45-B may have further enhanced glass hydrophobicity of the MS, thus possibly affecting the cell−material interaction. Moreover, the effect of released Fe ions, which could not be measured here, may add further useful information on the cellular response to the P45 material.

## 5. CONCLUSIONS

This study highlighted important changes occurring on PBG glass materials over extended periods of time and assessed how these could affect their biological performance for the support of MSCs in culture experiments for up to 6 weeks. The results demonstrated that the slowly degrading P45-B had low potential for cell expansion and osteogenic differentiation. By contrast, MSs made from the faster degrading P40, both in bulk and porous forms, represent better candidates for bone repair application, as they supported the formation of a bone-like matrix enriched with collagen, osteocalcin, and minerals deposited by MSCs. Surface delamination on these MSs as a result of glass degradation may be an important parameter to consider for their application in bone regeneration. Porosity in the P40 MS significantly enhanced the surface area (more than 10 times as compared to the bulk MS) and further enhanced the osteogenic response in terms of ALP activity and collagen production. However, glass fragments/particulates were observed in culture and negatively affected cells in culture. The presence of small pore windows on the P40-P surface may have further limited cell penetration into these MSs and could thus be optimized in future-generation materials. Additionally, different formulations of PBGs and annealing temperatures could be investigated to improve surface integrity over time, in order to limit the release of ions and particulates and enhance the therapeutic potential of these materials.

## ■ ASSOCIATED CONTENT

### Supporting Information

The Supporting Information is available free of charge at https://pubs.acs.org/doi/10.1021/acsabm.1c00120.

Summary of in vitro studies investigating different phosphate-based glass system degradation profiles and cytocompatibility over different time periods; parame-



https://doi.org/10.1021/acsabm.1c00120
ACS Appl. Bio Mater. 2021, 4, 5987−6004

ters for micro-computational tomography; measurements of atomic % via XPS on 3D aggregates after 14 and 21 days of culture; method for cytotoxicity experiments; identification of particles using ImageJ; identification of pore windows using ImageJ; methodology for quantification of MSs with apparent cracks and peeling surfaces; Ba loading in cells; cumulative frequency distribution of MAL of all MS types; internal pore structure of P40-P using Cryo-FIB SEM; BET surface area, relative density, tapped density, and normalized tapped density measurements of MSs; EDS analysis showing retention of the Ca-based porogen in P40-P; degradation of MSs in water analyzed using SEM and ESEM; effect of degradation products of MSs on hMSC growth; floating glass particulates in P40-B spent medium and P40-P spent media after 21 days; and representative wide scans for XPS analysis (PDF)

## AUTHOR INFORMATION


### Corresponding Authors

**Virginie Sottile** − *Wolfson Centre for Stem Cells, Tissue Engineering and Modelling (STEM), School of Medicine, University of Nottingham, Nottingham NG7 2RD, U.K.; Department of Molecular Medicine, University of Pavia, 27100 Pavia, Italy;* orcid.org/0000-0002-6064-5738; Email: virginie.sottile@unipv.it

**David M. Grant** − *Advanced Materials Research Group, Faculty of Engineering, University of Nottingham, Nottingham NG7 2RD, U.K.*; Email: david.grant@nottingham.ac.uk

### Authors

**Dhanak Gupta** − *Wolfson Centre for Stem Cells, Tissue Engineering and Modelling (STEM), School of Medicine, University of Nottingham, Nottingham NG7 2RD, U.K.; Advanced Materials Research Group, Faculty of Engineering, University of Nottingham, Nottingham NG7 2RD, U.K.;* Present Address: School of Dentistry, University of Birmingham, 5 Mill Pool Way, Edgbaston, Birmingham, B5 7EG, UK.; orcid.org/0000-0002-6493-1600

**Kazi M. Zakir Hossain** − *Advanced Materials Research Group, Faculty of Engineering, University of Nottingham, Nottingham NG7 2RD, U.K.;* Present Address: Department of Chemistry, University of Bath, Claverton Down, Bath, BA2 7AY.; orcid.org/0000-0002-4178-7271

**Martin Roe** − *Nanoscale & Microscale Research Centre, University of Nottingham, Nottingham NG7 2RD, U.K.*

**Emily F. Smith** − *Nanoscale & Microscale Research Centre and School of Chemistry, University of Nottingham, Nottingham NG7 2RD, U.K.*

**Ifty Ahmed** − *Advanced Materials Research Group, Faculty of Engineering, University of Nottingham, Nottingham NG7 2RD, U.K.*

Complete contact information is available at: https://pubs.acs.org/10.1021/acsabm.1c00120


### Author Contributions

D.G.: data curation, writing the original draft, methodology, formal analysis, validation, investigation, and funding acquisition. K.M.Z.H.: writing, review, editing, and methodology. M.R.: methodology, data curation, writing, review, and editing. E.F.S.: methodology, data curation, writing, review, and editing. I.A.: conceptualization, resources, writing, review, and editing. V.S.: conceptualization, validation, resources, visualization, supervision, writing, project administration, and funding acquisition. D.M.G.: conceptualization, validation, resources, visualization, supervision, writing, project administration, and funding acquisition.


### Funding

D.G. was supported by Vice Chancellor's Scholarship for Excellence in Research from the University of Nottingham. This work also received support from the European Union's Seventh Framework Programme (FP7/2007-2013) under grant agreement no. 263363. This work was supported by the Engineering and Physical Sciences Research Council [grant EP/K005138/1]. V.S. is supported by a grant from the Italian Ministry of Education, University and Research (MIUR) to the Department of Molecular Medicine of the University of Pavia under the initiative "Dipartimenti di Eccellenza (2018−2022)".


### Notes

The authors declare no competing financial interest.

## ACKNOWLEDGMENTS

We thank Dr Colin Scotchford (University of Nottingham) for valuable discussions, Nicola Weston (University of Nottingham) for expert advice on environmental SEM, Dr. Christopher Parmenter for assistance with Cryo-FIB SEM (Nanoscale and Microscale Research Centre, University of Nottingham), and Dr. Lee Stevens (Energy Technologies Building, University of Nottingham) for BET. The authors would like to thank the Nanoscale and Microscale Research Centre (nmRC) for providing access to instrumentation.

## ABBREVIATIONS

MSs, microspheres; ALP, alkaline phosphatase; PBG, phosphate based-glass; P45-B, P45 bulk; P40-B, P40 bulk; P40-P, P40 porous; BSG, borosilicate glass; SEM, scanning electron microscopy; ESEM, environmental SEM; EDS, energy-dispersive X-ray spectroscopy; XPS, X-ray photoelectron spectroscopy; CT, computational tomography; ECM, extracellular matrix; hMSC, human mesenchymal stem cells; NR, Neutral Red; PBS, phosphate saline buffer

## REFERENCES


(1) Dong, J.; Kojima, H.; Uemura, T.; Kikuchi, M.; Tateishi, T.; Tanaka, J. In Vivo Evaluation of a Novel Porous Hydroxyapatite to Sustain Osteogenesis of Transplanted Bone Marrow-Derived Osteoblastic Cells. *J. Biomed. Mater. Res.* **2001**, *57*, 208−216.

(2) Trounson, A.; McDonald, C. Stem Cell Therapies in Clinical Trials: Progress and Challenges. *Cell Stem Cell* **2015**, *17*, 11−22.

(3) Jaiswal, N.; Haynesworth, S. E.; Caplan, A. I.; Bruder, S. P. Osteogenic Differentiation of Purified, Culture-Expanded Human Mesenchymal Stem Cells in Vitro. *J. Cell. Biochem.* **1997**, *64*, 295−312.

(4) Wittkowske, C.; Reilly, G. C.; Lacroix, D.; Perrault, C. M. In Vitro Bone Cell Models: Impact of Fluid Shear Stress on Bone Formation. *Front. Bioeng. Biotechnol.* **2016**, *4*, 87.

(5) Chen, J.; Liu, R.; Yang, Y.; Li, J.; Zhang, X.; Li, J.; Wang, Z.; Ma, J. The Simulated Microgravity Enhances the Differentiation of Mesenchymal Stem Cells into Neurons. *Neurosci. Lett.* **2011**, *505*, 171−175.

(6) Ripamonti, U. Biomimetism, Biomimetic Matrices and the Induction of Bone Formation. *J. Cell. Mol. Med.* **2009**, *13*, 2953−2972.
(7) Chang, Y.-S.; Gu, H.-O.; Kobayashi, M.; Oka, M. Influence of Various Structure Treatments on Histological Fixation of Titanium Implants. *Jt. Arthroplasty* **1998**, *13*, 816−825.
(8) Karageorgiou, V.; Kaplan, D. Porosity of 3D Biomaterial Scaffolds and Osteogenesis. *Biomaterials* **2005**, *26*, 5474−5491.
(9) McBeath, R.; Pirone, D. M.; Nelson, C. M.; Bhadriraju, K.; Chen, C. S. Cell Shape, Cytoskeletal Tension, and RhoA Regulate Stem Cell Lineage Commitment. *Dev. Cell* **2004**, *6*, 483−495.
(10) Bidan, C. M.; Kommareddy, K. P.; Rumpler, M.; Kollmannsberger, P.; Fratzl, P.; Dunlop, J. W. C. Geometry as a Factor for Tissue Growth: Towards Shape Optimization of Tissue Engineering Scaffolds. *Adv. Healthcare Mater.* **2013**, *2*, 186−194.
(11) Jones, J. R. Review of Bioactive Glass: From Hench to Hybrids. *Acta Biomater.* **2013**, *9*, 4457−4486.
(12) Fu, Q.; Rahaman, M. N.; Bal, B. S.; Kuroki, K.; Brown, R. F. In Vivo Evaluation of 13-93 Bioactive Glass Scaffolds with Trabecular and Oriented Microstructures in a Subcutaneous Rat Implantation Model. *J. Biomed. Mater. Res., Part A* **2010**, *95*, 235−244.
(13) Knowles, J. C. Phosphate Based Glasses for Biomedical Applications. *J. Mater. Chem.* **2003**, *13*, 2395−2401.
(14) Rho, J.-Y.; Kuhn-Spearing, L.; Zioupos, P. Mechanical Properties and the Hierarchical Structure of Bone. *Med. Eng. Phys.* **1998**, *20*, 92−102.
(15) Hasan, M. S.; Ahmed, I.; Parsons, A. J.; Walker, G. S.; Scotchford, C. A. Material Characterisation and Cytocompatibility Assessment of Quinternary Phosphate Glasses. *J. Mater. Sci.: Mater. Med.* **2012**, *23*, 2531−2541.
(16) Hossain, K. M. Z.; Patel, U.; Kennedy, A. R.; Macri-Pellizzeri, L.; Sottile, V.; Grant, D. M.; Scammell, B. E.; Ahmed, I. Porous Calcium Phosphate Glass Microspheres for Orthobiologic Applications. *Acta Biomater.* **2018**, *72*, 396−406.
(17) Skelton, K.; Glenn, J.; Clarke, S.; Georgiou, G.; Valappil, S.; Knowles, J.; Nazhat, S.; Jordan, G. Effect of Ternary Phosphate-Based Glass Compositions on Osteoblast and Osteoblast-like Proliferation, Differentiation and Death in Vitro. *Acta Biomater.* **2007**, *3*, 563−572.
(18) Neel, E. A. A.; O'Dell, L. A.; Chrzanowski, W.; Smith, M. E.; Knowles, J. C. Control of Surface Free Energy in Titanium Doped Phosphate Based Glasses by Co-Doping with Zinc. *J. Biomed. Mater. Res., Part B* **2009**, *89*, 392−407.
(19) Abou Neel, E. A.; Chrzanowski, W.; Valappil, S. P.; O'Dell, L. A.; Pickup, D. M.; Smith, M. E.; Newport, R. J.; Knowles, J. C. Doping of a High Calcium Oxide Metaphosphate Glass with Titanium Dioxide. *J. Non-Cryst. Solids* **2009**, *355*, 991−1000.
(20) Abou Neel, E. A.; Chrzanowski, W.; Knowles, J. C. Biological Performance of Titania Containing Phosphate-Based Glasses for Bone Tissue Engineering Applications. *Mater. Sci. Eng. C* **2014**, *35*, 307−313.
(21) Sharmin, N.; Hasan, M. S.; Parsons, A. J.; Furniss, D.; Scotchford, C. A.; Ahmed, I.; Rudd, C. D. Effect of Boron Addition on the Thermal, Degradation, and Cytocompatibility Properties of Phosphate-Based Glasses. *BioMed Res. Int.* **2013**, *2013*, 902427.
(22) Shah Mohammadi, M.; Chicatun, F.; Stähli, C.; Muja, N.; Bureau, M. N.; Nazhat, S. N. Osteoblastic Differentiation under Controlled Bioactive Ion Release by Silica and Titania Doped Sodium-Free Calcium Phosphate-Based Glass. *Colloids Surf., B* **2014**, *121*, 82−91.
(23) Abou Neel, E. A.; Knowles, J. C. Physical and Biocompatibility Studies of Novel Titanium Dioxide Doped Phosphate-Based Glasses for Bone Tissue Engineering Applications. *J. Mater. Sci.: Mater. Med.* **2008**, *19*, 377−386.
(24) Franks, K.; Salih, V.; Knowles, J. C.; Olsen, I. The Effect of MgO on the Solubility Behavior and Cell Proliferation in a Quaternary Soluble Phosphate Based Glass System. *J. Mater. Sci.: Mater. Med.* **2002**, *13*, 549−556.
(25) Abou Neel, E. A.; Chrzanowski, W.; Knowles, J. C. Effect of Increasing Titanium Dioxide Content on Bulk and Surface Properties of Phosphate-Based Glasses. *Acta Biomater.* **2008**, *4*, 523−534.
(26) Patel, U.; Moss, R. M.; Hossain, K. M. Z.; Kennedy, A. R.; Barney, E. R.; Ahmed, I.; Hannon, A. C. Structural and Physico-Chemical Analysis of Calcium/Strontium Substituted, near-Invert Phosphate Based Glasses for Biomedical Applications. *Acta Biomater.* **2017**, *60*, 109−127.
(27) Patel, U.; Macri-Pellizzeri, L.; Zakir Hossain, K. M.; Scammell, B. E.; Grant, D. M.; Scotchford, C. A.; Hannon, A. C.; Kennedy, A. R.; Barney, E. R.; Ahmed, I.; Sottile, V. In Vitro Cellular Testing of Strontium/Calcium Substituted Phosphate Glass Discs and Microspheres Shows Potential for Bone Regeneration. *J. Tissue Eng. Regener. Med.* **2019**, *13*, 396−405.
(28) Franks, K.; Abrahams, I.; Knowles, J. C. Development of Soluble Glasses for Biomedical Use Part I: In Vitro Solubility Measurement. *J. Mater. Sci.: Mater. Med.* **2000**, *11*, 609−614.
(29) Salih, V.; Franks, K.; James, M.; Hastings, G. W.; Knowles, J. C.; Olsen, I. Development of Soluble Glasses for Biomedical Use Part II: The Biological Response of Human Osteoblast Cell Lines to Phosphate-Based Soluble Glasses. *J. Mater. Sci.: Mater. Med.* **2000**, *11*, 615−620.
(30) Brauer, D. S.; Rüssel, C.; Li, W.; Habelitz, S. Effect of Degradation Rates of Resorbable Phosphate Invert Glasses on in Vitro Osteoblast Proliferation. *J. Biomed. Mater. Res., Part A* **2006**, *77*, 213−219.
(31) Parsons, A. J.; Evans, M.; Rudd, C. D.; Scotchford, C. A. Synthesis and Degradation of Sodium Iron Phosphate Glasses and Their in Vitro Cell Response. *J. Biomed. Mater. Res., Part A* **2004**, *71*, 283−291.
(32) Lakhkar, N. J.; Abou Neel, E. A.; Salih, V.; Knowles, J. C. Strontium Oxide Doped Quaternary Glasses: Effect on Structure, Degradation and Cytocompatibility. *J. Mater. Sci.: Mater. Med.* **2009**, *20*, 1339−1346.
(33) Lakhkar, N. J.; Park, J.-H.; Mordan, N. J.; Salih, V.; Wall, I. B.; Kim, H.-W.; King, S. P.; Hanna, J. V.; Martin, R. A.; Addison, O.; Mosselmans, J. F. W.; Knowles, J. C. Titanium Phosphate Glass Microspheres for Bone Tissue Engineering. *Acta Biomater.* **2012**, *8*, 4181−4190.
(34) Lakhkar, N. J.; Day, R.; Kim, H.-W.; Ludka, K.; Mordan, N. J.; Salih, V.; Knowles, J. C. Titanium Phosphate Glass Microcarriers Induce Enhanced Osteogenic Cell Proliferation and Human Mesenchymal Stem Cell Protein Expression. *J. Tissue Eng.* **2015**, *6*, 204173141561774.
(35) Abou Neel, E. A.; Mizoguchi, T.; Ito, M.; Bitar, M.; Salih, V.; Knowles, J. C. In Vitro Bioactivity and Gene Expression by Cells Cultured on Titanium Dioxide Doped Phosphate-Based Glasses. *Biomaterials* **2007**, *28*, 2967−2977.
(36) Navarro, M.; Valle, S. d.; Martínez, S.; Zeppetelli, S.; Ambrosio, L.; Planell, J. A.; Ginebra, M. P. New Macroporous Calcium Phosphate Glass Ceramic for Guided Bone Regeneration. *Biomaterials* **2004**, *25*, 4233−4241.
(37) McLaren, J. S.; Macri-Pellizzeri, L.; Hossain, K. M. Z.; Patel, U.; Grant, D. M.; Scammell, B. E.; Ahmed, I.; Sottile, V. Porous Phosphate-Based Glass Microspheres Show Biocompatibility, Tissue Infiltration, and Osteogenic Onset in an Ovine Bone Defect Model. *ACS Appl. Mater. Interfaces* **2019**, *11*, 15436−15446.
(38) Gupta, D.; Grant, D. M.; Zakir Hossain, K. M.; Ahmed, I.; Sottile, V. Role of Geometrical Cues in Bone Marrow-Derived Mesenchymal Stem Cell Survival, Growth and Osteogenic Differentiation. *J. Biomater. Appl.* **2018**, *32*, 906−919.
(39) Gupta, D.; Hossain, K. M. Z.; Ahmed, I.; Sottile, V.; Grant, D. M. Flame-Spheroidized Phosphate-Based Glass Particles with Improved Characteristics for Applications in Mesenchymal Stem Cell Culture Therapy and Tissue Engineering. *ACS Appl. Mater. Interfaces* **2018**, *10*, 25972−25982.
(40) Harrison, R.; Markides, H.; Morris, R. H.; Richards, P.; El Haj, A. J.; Sottile, V. Autonomous Magnetic Labelling of Functional Mesenchymal Stem Cells for Improved Traceability and Spatial


https://doi.org/10.1021/acsabm.1c00120
*ACS Appl. Bio Mater.* 2021, 4, 5987−6004

Control in Cell Therapy Applications. *J. Tissue Eng. Regener. Med.* **2017**, *11*, 2333−2348.
(41) *ISO 10993−12:2009. Biological Evaluation of Medical Devices—Part 12: Sample Preparation and Reference Materials*, 2009.
(42) *ISO 10993−5:2009. Biological Evaluation of Medical Devices—Part 5: Tests for in Vitro Cytotoxicity*, 2009.
(43) McArthur, S. L.; Mishra, G.; Easton, C. D. *Applications of XPS in Biology and Biointerface Analysis BT—Surface Analysis and Techniques in Biology*; Smentkowski, V. S., Ed.; Springer International Publishing: Cham, 2014; pp 9−36.
(44) Chakrabarti, A. C.; Veiro, J. A.; Wong, N. S.; Wheeler, J. J.; Cullis, P. R. Generation and Characterization of Iron- and Barium-Loaded Liposomes. *Biochim. Biophys. Acta, Biomembr.* **1992**, *1108*, 233−239.
(45) Demri, B.; Muster, D. XPS Study of Some Calcium Compounds. *J. Mater. Process. Technol.* **1995**, *55*, 311−314.
(46) Tsigkou, O.; Labbaf, S.; Stevens, M. M.; Porter, A. E.; Jones, J. R. Monodispersed Bioactive Glass Submicron Particles and Their Effect on Bone Marrow and Adipose Tissue-Derived Stem Cells. *Adv. Healthcare Mater.* **2014**, *3*, 115−125.
(47) Labbaf, S.; Tsigkou, O.; Müller, K. H.; Stevens, M. M.; Porter, A. E.; Jones, J. R. Spherical Bioactive Glass Particles and Their Interaction with Human Mesenchymal Stem Cells in Vitro. *Biomaterials* **2011**, *32*, 1010−1018.
(48) Choueka, J.; Charvet, J. L.; Alexander, H.; Oh, Y. H.; Joseph, G.; Blumenthal, N. C.; LaCourse, W. C. Effect of Annealing Temperature on the Degradation of Reinforcing Fibers for Absorbable Implants. *J. Biomed. Mater. Res.* **1995**, *29*, 1309−1315.
(49) Lakhkar, N. J. *Phosphate Glass Microspheres as Cell Microcarrier Substrates for Bone Tissue Engineering Applications*; University College London, 2014.
(50) Parsons, A. J.; Ahmed, I.; Haque, P.; Fitzpatrick, B.; Niazi, M. I. K.; Walker, G. S.; Rudd, C. D. Phosphate Glass Fibre Composites for Bone Repair. *J. Bionic Eng.* **2009**, *6*, 318−323.
(51) Gough, J. E.; Jones, J. R.; Hench, L. L. Nodule Formation and Mineralisation of Human Primary Osteoblasts Cultured on a Porous Bioactive Glass Scaffold. *Biomaterials* **2004**, *25*, 2039−2046.
(52) Brown, R. B.; Razzaque, M. S. Dysregulation of Phosphate Metabolism and Conditions Associated with Phosphate Toxicity. *BoneKEy Rep.* **2015**, *4*, 1−7.
(53) Di Marco, G. S.; Hausberg, M.; Hillebrand, U.; Rustemeyer, P.; Wittkowski, W.; Lang, D.; Pavenstädt, H. Increased Inorganic Phosphate Induces Human Endothelial Cell Apoptosis in Vitro. *Am. J. Physiol.* **2008**, *294*, F1381−F1387.
(54) Liu, Y. K.; Lu, Q. Z.; Pei, R.; Ji, H. J.; Zhou, G. S.; Zhao, X. L.; Tang, R. K.; Zhang, M. The Effect of Extracellular Calcium and Inorganic Phosphate on the Growth and Osteogenic Differentiation of Mesenchymal Stem Cells in Vitro: Implication for Bone Tissue Engineering. *Biomed. Mater.* **2009**, *4*, 025004.
(55) Dalby, M. J.; Gadegaard, N.; Tare, R.; Andar, A.; Riehle, M. O.; Herzyk, P.; Wilkinson, C. D. W.; Oreffo, R. O. C. The Control of Human Mesenchymal Cell Differentiation Using Nanoscale Symmetry and Disorder. *Nat. Mater.* **2007**, *6*, 997−1003.
(56) Park, J. Y.; Lee, D. H.; Lee, E. J.; Lee, S.-H. Study of Cellular Behaviors on Concave and Convex Microstructures Fabricated from Elastic PDMS Membranes. *Lab Chip* **2009**, *9*, 2043−2049.
(57) Fischer, E. M.; Layrolle, P.; Van Blitterswijk, C. A.; de Bruijn, J. D. Bone Formation by Mesenchymal Progenitor Cells Cultured on Dense and Microporous Hydroxyapatite Particles. *Tissue Eng.* **2003**, *9*, 1179−1188.
(58) Elliott, H.; Fischer, R. S.; Myers, K. A.; Desai, R. A.; Gao, L.; Chen, C. S.; Adelstein, R. S.; Waterman, C. M.; Danuser, G. Myosin II Controls Cellular Branching Morphogenesis and Migration in Three Dimensions by Minimizing Cell-Surface Curvature. *Nat. Cell Biol.* **2015**, *17*, 137−147.
(59) Binamé, F.; Pawlak, G.; Roux, P.; Hibner, U. What Makes Cells Move: Requirements and Obstacles for Spontaneous Cell Motility. *Mol. BioSyst.* **2010**, *6*, 648−661.
(60) Berry, C.; Dalby, M.; McCloy, D.; Affrossman, S. The Fibroblast Response to Tubes Exhibiting Internal Nanotopography. *Biomaterials* **2005**, *26*, 4985−4992.
(61) Taylor, A. F. Osteoblastic Glutamate Receptor Function Regulates Bone Formation and Resorption. *J. Musculoskeletal Neuronal Interact.* **2002**, *2*, 285−290.
(62) Valerio, P.; Pereira, M. M.; Goes, A. M.; Leite, M. F. Effects of Extracellular Calcium Concentration on the Glutamate Release by Bioactive Glass (BG60S) Preincubated Osteoblasts. *Biomed. Mater.* **2009**, *4*, 045011.
(63) Barrias, C. C.; Ribeiro, C. C.; Lamghari, M.; Miranda, C. S.; Barbosa, M. r. A. Proliferation, Activity, and Osteogenic Differentiation of Bone Marrow Stromal Cells Cultured on Calcium Titanium Phosphate Microspheres. *J. Biomed. Mater. Res., Part A* **2005**, *72*, 57−66.
(64) Gao, P.; Zhang, H.; Liu, Y.; Fan, B.; Li, X.; Xiao, X.; Lan, P.; Li, M.; Geng, L.; Liu, D.; Yuan, Y.; Lian, Q.; Lu, J.; Guo, Z.; Wang, Z. Beta-Tricalcium Phosphate Granules Improve Osteogenesis in Vitro and Establish Innovative Osteo-Regenerators for Bone Tissue Engineering in Vivo. *Sci. Rep.* **2016**, *6*, 23367.
(65) Wilkinson, A.; Hewitt, R. N.; McNamara, L. E.; McCloy, D.; Dominic Meek, R. M.; Dalby, M. J. Biomimetic Microtopography to Enhance Osteogenesis in Vitro. *Acta Biomater.* **2011**, *7*, 2919−2925.
(66) Bidan, C. M.; Kollmannsberger, P.; Gering, V.; Ehrig, S.; Joly, P.; Petersen, A.; Vogel, V.; Fratzl, P.; Dunlop, J. W. C. Gradual Conversion of Cellular Stress Patterns into Prestressed Matrix Architecture during In-Vitro Tissue Growth. *J. R. Soc., Interface* **2016**, *13*, 20160136.
(67) Yu, X.; Day, D. E.; Long, G. J.; Brow, R. K. Properties and Structure of Sodium-Iron Phosphate Glasses. *J. Non-Cryst. Solids* **1997**, *215*, 21−31.
(68) Abou Neel, E. A.; Ahmed, I.; Blaker, J. J.; Bismarck, A.; Boccaccini, A. R.; Lewis, M. P.; Nazhat, S. N.; Knowles, J. C. Effect of Iron on the Surface, Degradation and Ion Release Properties of Phosphate-Based Glass Fibres. *Acta Biomater.* **2005**, *1*, 553−563.


https://doi.org/10.1021/acsabm.1c00120
*ACS Appl. Bio Mater.* 2021, 4, 5987−6004